International Journal of Heat and Mass Transfer 108 (2017) 2303–2320

Contents lists available at ScienceDirect

International Journal of Heat and Mass Transfer

journal homepage: www.elsevier.com/locate/ijhmt

Review

Infrared imaging technology for breast cancer detection – Current status, protocols and new directions

Satish G. Kandlikar [a,*], Isaac Perez-Raya [a], Pruthvik A. Raghupathi [a], Jose-Luis Gonzalez-Hernandez [a], Donnette Dabydeen [b], Lori Medeiros [c], Pradyumna Phatak [d]

[a] Department of Mechanical Engineering, Rochester Institute of Technology, 76 Lomb Memorial Drive, Rochester, NY 14623, USA
[b] Department of Radiology, Rochester General Hospital Regional, 1425 Portland Avenue, Rochester, NY 14621, USA
[c] Rochester General Breast Center, Rochester, 1425 Portland Avenue, Rochester, NY 14621, USA
[d] Department of Medicine and Lipson Cancer Institute, Rochester General Hospital, 1425 Portland Avenue, Rochester, NY 14621, USA

ARTICLE INFO

Article history:
Received 8 November 2016
Received in revised form 17 January 2017
Accepted 21 January 2017
Available online 6 February 2017

Keywords:
Thermal imaging
Breast cancer
Inverse modeling
Bioheat modeling
Thermography

ABSTRACT

Early and accurate detection of breast cancer is a critical part of the strategy to reduce the morbidity and mortality associated with this common disease. While current guidelines recommend mammography for screening, the sensitivity and specificity of mammograms remains less than optimal, especially for patients with dense breast tissue. Thermography has been explored in the past as an alternative to mammography. Advances in IR cameras that are used to obtain thermal images of the breast as well as computational tools used to accurately model heat transfer within the breast have significantly increased the accuracy of thermography. The current work reviews the progress that has been made in using thermal imaging to detect breast cancer over the past three decades and identifies aspects that need further refinement for it to become a reliable tool to diagnose breast cancer. Recent advances and suggestions for future work in the field including using advanced simulation methods, inverse modeling, imaging protocols, and using artificial neural networks to better predict the location of the tumor are also presented.

Contents

* Corresponding author.
E-mail addresses: sgkeme@rit.edu (S.G. Kandlikar), ibp1401@rit.edu (I. Perez-Raya), par3002@rit.edu (P.A. Raghupathi), jxg4140@rit.edu (J.-L. Gonzalez-Hernandez), bDonnette.Dabydeen@rochesterregional.org (D. Dabydeen), Lori.Medeiros@rochesterregional.org (L. Medeiros), Pradyumna.Phatak@rochesterregional.org (P. Phatak).

http://dx.doi.org/10.1016/j.ijheatmasstransfer.2017.01.086
0017-9310/

1. Introduction

The term cancer is used to describe a group of disorders associated with dysregulated cell growth leading to tumor formation, invasion into surrounding tissues and spread to other parts of the body. Some of the most common types of cancer originate in the breast, prostate, lung, skin and pancreas. The exact reasons for developing cancer have not been determined [1,2]. However researchers agree that factors such as genetic predisposition, age, smoking tobacco, exposure to ultraviolet radiation, unhealthy lifestyle, and exposure to carcinogenic agents can significantly increase the odds of a person being affected by cancer. Between 2008 and 2010, the average annual cost of healthcare for a newly diagnosed cancer patient in the US was $ 21,222 [3]. The economic impact due to loss in productivity by cancer in the US was estimated to be $130 billion in 2009 alone [4]. By 2020 the cost of cancer treatment is expected to reach $158 billion just in the US [5]. Over the past few decades a large amount of research has emphasized on improving diagnostic techniques used to detect cancer at an early stage when treatment can be less expensive and more effective.

Breast cancer is the most frequently diagnosed form of cancer among women and has the second highest mortality rate after skin cancer. It is estimated that the lifetime probability of being diagnosed with invasive breast cancer among women is 12.3% with 246,660 women expected to be diagnosed with breast cancer in the United States in 2016 [6]. A healthy breast consists of glands that are connected to the surface of the skin by ducts. The glands and ducts are surrounded by connective tissue embedded in which are blood vessels, lymph nodes, lymph channels and nerves. Breast cancer can originate in any part of the breast with more than 20 types of cancer having been identified. The most common types of breast cancer are ductal carcinoma, which originates in the ductal epithelium; and lobular carcinoma, which develops in the glands.

Sensitivity of a diagnostic technique is a measure of the rate at which a tumor is detected by the technique. Specificity of a technique refers to the accuracy of a positive diagnosis. Higher the sensitivity, greater is the likelihood of a tumor in a patient being detected, and higher the specificity, greater is the probability of a positive diagnosis of being true. A variety of imaging modalities aimed at improving the sensitivity and specificity for breast cancer detection have been developed. Mammography however remains the mainstay of screening for breast cancer. Supplemental screening and diagnostic techniques for breast cancer detection include ultrasound, Magnetic Resonance Imaging (MRI), and tomosynthesis. No single imaging modality is capable of identifying and characterizing all breast abnormalities and a combined modality approach is still necessary.

Mammography it the most common screening technique which detects the presence of a tumor using low energy X-rays to image the internal anatomy of the breast. Mammography detects masses in the breast and calcifications, which may indicate the presence of a tumor. A randomized trial with 134,867 women aged between 40 and 74 showed that regular screening resulted in a 31% reduction in mortality from breast cancer [7]. However, the rate of false positives using mammograms is high with a 10 year study showing that the likelihood of a false positive diagnosis for women after getting a mammogram every year for 10 years to be 49.1% [8]. Mammography is also known to be less sensitive for women with dense breast tissue, since the cancer can be obscured or masked by the normal surrounding fibroglandular tissue; the greater the ratio of fibroglandular tissue to fat in the breast, the greater the density of the breast. Approximately 50% of women undergoing screening mammography have dense breasts. The proportion of the glandular tissue is higher for younger women and fat content in the breast increases as women get older. Kerlikowske et al. [9] studied the effect of breast density and age on the sensitivity of mammography and found that the technique has the high sensitivity for women 50 years or older due to increased fatty tissue content while the sensitivity was relatively lower for women under 50 due the denser breast tissue.

MRI uses a strong magnetic field along with pulsing radio waves to get a high resolution image of the breast at different cross-sections. A contrast agent is added to help better image the breast. This procedure is used to screen women who are at a high risk of developing breast cancer or to better image tumors found in other tests [10]. This procedure is very expensive and time consuming and hence is only used as an adjunct to mammography for high risk asymptomatic and symptomatic women. Screening breast MRI has been found to be more sensitive but less specific than mammography for the detection of invasive breast cancers in high-risk women in both retrospective and prospective studies [11,12].

Ultrasound or sonography detects the presence of tumors by bouncing sound waves of the surface of the tissue. A transducer is used to interpret the reflected sound waves in order to determine the boundaries of different types of tissue. This technique is normally used to further investigate suspicious areas of the breast found in the mammogram or during a breast exam. It can help distinguish between cysts (non-tumorous sacks filled with fluid) and solid masses. It is also used for supplemental screening in subsets of patients with dense breasts. When used as a supplement to mammography, ultrasound can improve sensitivity of screening at the expense of decreased specificity and increased biopsy rate [13]. Ultrasound is an attractive supplement to mammography because it is widely available, relatively inexpensive and does not inconvenience the patients.

Digital breast tomosynthesis, also known as 3D mammography, provides three-dimensional images using a moving X-ray source and digital detector. Tomosynthesis has been approved in the United States for breast cancer screening, when used in combination with mammography. Tomosynthesis, when used in combination with mammography have been shown to modestly increase the

Table 1
Comparison of imaging techniques for breast cancer.

Technique	Mechanism of operation	Sensitivity	Specificity	Cost	Method	Cause of discomfort	Recommended for
Mammography	Low energy X-rays	84%	92%	Moderate	Compressed breast	Pain from breast compression	Screening and diagnostic evaluation
Magnetic Resonance Imaging (MRI)	Magnetic field and pulsating radio waves	90%	50%	High	IV contrast injected and dynamic images obtained	Claustrophobia Holding still and lying prone for a long exam Possible reaction to contrast agent Contrast cannot be used in patients with renal insufficiency	Screening in women at high risk for breast cancer Diagnostic evaluation
Positron Emission Tomography (PET)	Gamma rays emitted by tracer substance	90%	86%	High	Small amount of radioactive tracer injected in the body	No significant discomfort	Determine if cancer has spread to other parts of the body
Ultrasound	High frequency sound waves	82%	84%	Low	Hand-held or automated ultrasound device	No significant discomfort	Screening in women with dense breasts Diagnostic evaluation
Tomosynthesis (3D mammography)						Low energy X-rays	90%
	Moderate				Compressed breast	Pain from breast compression	Screening and diagnostic evaluation
Electronic Palpation Imaging (EPI)	Pressure changes	84%	82%	Low	Hand-held electronic tactile sensor	Small localized pressure	Follow-up after abnormal finding
Electrical Impedance Scanning	Electrical impedance	87%	82%	Low	Electrodes attached to skin	Small alternating currents applied to the electrodes	Follow-up after abnormal finding

cancer detection rate and decreases false positives mammography readings, when compared to mammography alone [14]. Tomosynthesis is typically performed in conjunction with conventional mammogram, which increases the patient radiation exposure by two fold. However, the increased total dose is still below the FDA safety limits. Software has been developed to reconstruct the digital mammogram from the 3D dataset, lowering the radiation dose to levels comparable to a conventional mammogram.

Over the last few decades, the need for cheap and effective diagnostic techniques to screen and diagnose breast cancer have led to the development of various new technologies. Three recent techniques that have emerged are electronic palpation imaging, electrical impedance scanning (EIS), and thermal imaging. Electronic palpation imaging (EPI) detects the presence of a tumor in the breast by generating a map of the rigidity of the breast tissue by imposing pressure waves and observing the resultant displacement of different regions of the breast [15]. The second method that has been developed over the years is electrical impedance scanning which, as the name suggests, measures the electrical impedance of the breast to detect the presence of tumors. The electrical conductivity of the tumor is higher than that of healthy breast tissue and therefore, the electrical impedance is lower than the healthy tissue. Thermal techniques such as Liquid Crystal Thermography and Infrared (IR) imaging rely on surface temperature readings of the breast. Since tumors are clusters of cells which multiply in an uncontrolled manner, the metabolic heat generation rate and the blood perfusion rate of the tumor are higher than normal tissues. The increased heat generation at the tumor is dissipated to the surrounding tissue and can be seen as a temperature spike at the surface of the breast. Table 1 presents a comparison of the different imaging techniques for breast cancer.

Analyzing the change in the temperature at the surface of the breast can help predict the size and location of the tumor. Liquid crystal thermography was initially considered as a viable technique to measure the surface temperature of the breast with a sensitivity of about 0.1 °C. Liquid crystal thermography was widely used mainly due to the higher costs associated with non-contact IR camera. The major drawbacks of liquid crystal thermography are the need for contact between the breast and a film with the liquid crystals; the need for external light sources, that indeed can cause bias in the colors perceived [16]. Infrared thermography used an infrared camera to map the temperature of the breast to predict the presence of a tumor in the breast. This technique is superior to liquid crystal thermography since it does not require direct contact with the patient and does not introduce any bias as a result of the contact. With infrared cameras becoming dramatically better over the past few decades, infrared thermography has increasingly become an active field of research.

Vreugdenburg et al. [17] conducted a systematic study of the published clinical results using infrared thermography, electrical impedance scanning and electronic palpation imaging by identifying 5441 studies and reviewing the results of 60 publications. In case of infrared thermography it was seen that the sensitivity of infrared thermography was between 0.71 and 0.94 (with one outlier). However, the specificity of the technique was seen to be poor, varying from 0.14 to 0.85. Fig. 1 shows the sensitivity and specificity reported by some of the studies reviewed. The heterogeneity in the results reported was attributed to the wide range of devices used in these studies and the differences in the algorithm used to classify the IR thermograms as normal or diseased. Broadly, there is an inverse relationship between the sensitivity and specificity for IR thermography. Studies reporting high sensitivity appear to have a low threshold for classifying a thermogram as abnormal and therefore have poor specificity (e.g. Parisky et al. [18]), Tang et al. [19], Arora et al. [20]). Similarly, studies where the threshold for classifying a thermogram as abnormal is high, the sensitivity reported is low while the specificity is high (e.g. Kontos and Wilson [21]).

2. Breast Thermography

2.1. Infrared imaging

Infrared thermography works on the principle of measuring the radiation emitted by a surface to determine its temperature.

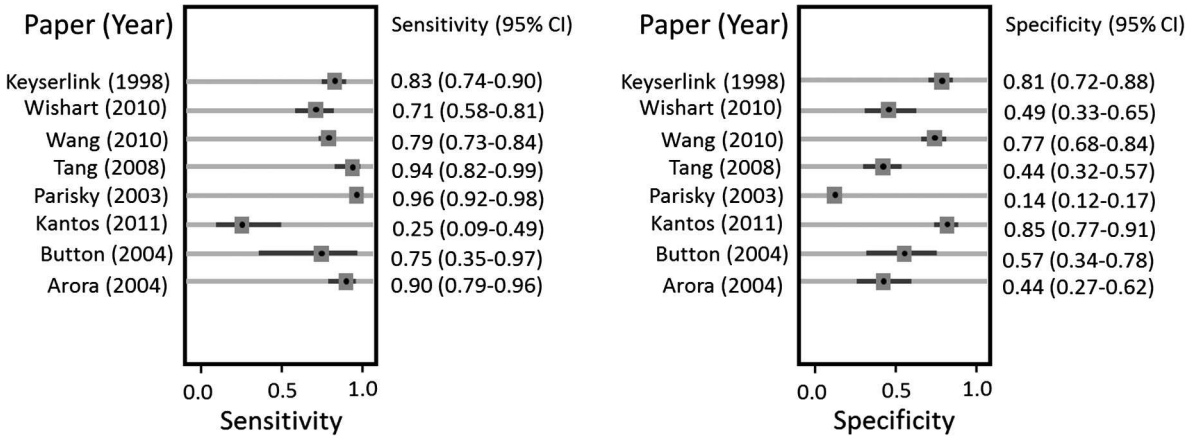

Fig. 1. Comparison of sensitivity and specificity from different clinical trials adapted from [17].

According to Planck's radiation law, any object above absolute zero temperature emits electromagnetic radiation whose spectrum and intensity is a function of the temperature of the body. The intensity of radiation (I) corresponding to a wavelength λ that an object at a temperature T emits is given by

$$I(\lambda, T) = \frac{2\pi hc^2}{\lambda^4}\left(e^{\frac{hc}{\lambda kT}} - 1\right)^{-1} \quad (1)$$

where h is the Planck constant, c is the speed of light in vacuum, and k is the Boltzmann constant. For an object at room temperature, most of the radiation emitted is in the infrared spectrum. Therefore by measuring the infrared radiation that an object emits, its temperature can be determined. The human body at normal temperatures mainly emits 10 μm wavelength with 90% of the total radiation in the 6–14 μm wavelength band.

In order to detect the infrared radiation the cameras need specialized lenses and sensors. Since glass that is used in traditional cameras absorbs infrared radiation, the lenses used in IR cameras are made of IR transparent materials such as Germanium or Sapphire. The sensors used to record the IR images are broadly classified into thermal detectors and quantum detectors. Uncooled microbolometers are the most common type of thermal detectors and are made of metal or semiconductor materials. These detectors have a broader IR spectral response but are significantly slower and less sensitive than quantum detectors. Cameras using uncooled sensors are smaller since they do not require a self-contained cooling system and thereby less expensive. The detectors in the advanced cameras are cooled to reduce the IR radiation emitted by itself that would otherwise affect its accuracy. The sensors are typically cooled to a temperature of 60–100 K using a various techniques including rotary sterling engine cryo-coolers and expansion of pressurized gas. The materials used to make the cooled sensors are narrow band gap semiconductors that are capable of detecting long infrared radiation. Some of the commonly used materials include Indium antimonide, Indium arsenide and mercury cadmium telluride.

The sensitivity of IR cameras to temperature variations has consistently been improving over the last four decades. Early generation IR cameras had a temperature sensitivity of about 0.3 K. Under such sensitivity, the most subtle temperature variations were not captured and the heat pattern obtained lacked fine details. With the improvement of IR detectors, modern IR cameras can achieve sensitivities below 0.02 K (20 mK). Such high degree of accuracy was possible due to the development of cooled quantum detectors (InSb). This dramatic improvement in sensitivity has allowed for the capture of more detailed thermograms that are able to detect small, localized temperature variations. Fig. 2 chronicles the improvement in the sensitivity of IR cameras over the last four decades.

Modern infrared cameras require a more stringent control on the environmental conditions to accurately measure temperature differences as low as 20 mK. Ng [22] recommends to minimize the sources of IR interference, such as windows; avoid sources of light such as incandescent, halogen or sunlight. A plain, non-reflective background is recommended and IR reflective surfaces should be covered to minimize undesired reflections.

Factors such as the emissivity of the skin can affect the temperature measured by the infrared camera. As infrared cameras became popular in the 60s, multiple studies focused on the emissivity of skin at different wavelengths. Early studies by Hardy [23] as well as subsequent studies conducted by Watmough and Oliver [24] measured skin emissivity at different infrared wavelengths. They concluded that the emissivity of the skin is independent of the wavelength and equal to 0.989 ± 0.01. Similar findings were also reported by Steketee [25] and Patil and Williams [26]. Therefore as long as standard operating procedures are followed, the temperature recorded by the infrared camera would be an accurate measurement of the actual skin temperature.

2.2. IR thermography to detect breast cancer

Lawson [27], in 1956 was one of the first researchers to report the use of surface temperature measurements as a possible tool for breast cancer diagnosis. Later in 1963, Lawson and Chugtai [28] used IR scanners to determine that the surface temperature of the region surrounding a tumor is about 2 °C higher than the surface temperature of the same region on the contralateral

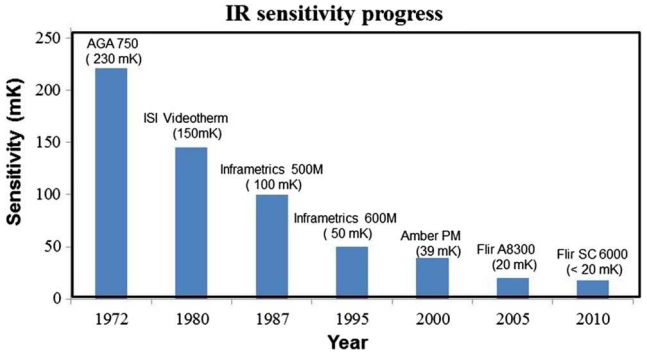

Fig. 2. Improvements in IR camera sensitivity over the years.

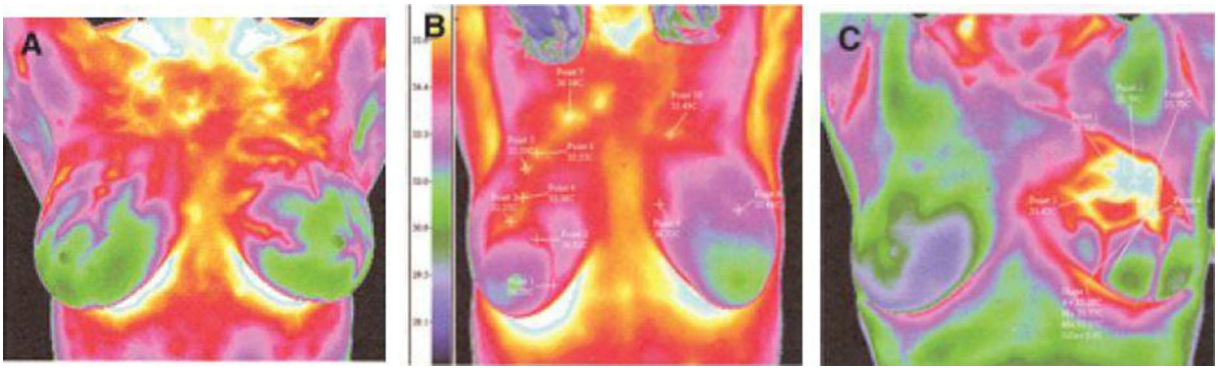

Fig. 3. Thermograms of (a) normal breast, (b) with early stages of cancer in the right breast, and (c) advanced cancer in the left breast [34].

healthy breast. Davison et al. [29] used liquid crystal thermography to measure the temperature of the breast of patients with cancer. They found that liquid crystal thermography and IR thermography produce similar results. In 1980, Gautherie [30] measured the internal temperature along a breast with a cancer tumor using a fine needle thermocouple. He found that the presence of a tumor resulted in a localized peak in tissue temperature. The temperature in the tumor was approximately 3 °C higher than the surface temperature at the same axis. These preliminary results showing a relationship between the temperature profile at the breast surface and presence of a malignant tumor lead to breast thermography being approved by the FDA as an adjunct tool to mammography for breast cancer detection in 1982.

During early stages of infrared thermography, the rate of true positive diagnoses was as low as 41%. This low accuracy was primarily due to the lack of standards concerning measuring conditions. Besides, most clinicians that used IR thermographs were not adequately trained in using IR cameras [31]. It wasn't until early 2000s that improvements in infrared cameras, and rapid advances in computing and simulation lead researchers to once again explore thermography as a screening tool to detect breast cancer. A more detailed historical perspective of IR thermography can be found in [31–33,22].

When there is an abnormality in the breast tissue such as a malignant tumor, fibrosis, an infection or an inflammation, there is an increase in the temperature at the surface of the breast. Fig. 3 shows the thermograms of three patients with (a) healthy breast, (b) early stage cancer in the right breast and (c) advanced cancer in the left breast [34]. Temperature in the vicinity of the affected tissue is about 2.5 °C higher than for normal tissue (contralateral unaffected region). The surface temperature distribution of tumorous breasts is affected by the size, position, depth and stage of the tumor. Hormone intake (contraceptive), pregnancy and lactation also have an effect on the breast temperature. In general, the tumor is more easily identified when it is shallow. For deep tumors, the surface temperature variation can be very subtle with respect to a healthy breast. For this reason, highly accurate infrared cameras as well as standardized techniques for IR screening are required [35].

Gautherie and Gross [33] reported the study of 1245 patients who were detected to have abnormal IR image profiles. They observed that IR imaging, besides to predict cancer, can identify rapidly growing neoplasms. Gautherie [32] found that 35% of the patients with abnormal thermograms developed cancer during the next 5 years; therefore they stated that IR thermography can predict the development of breast cancer. However, through IR thermograms is very difficult to distinguish between breast cancer and inflammation zones.

2.2.1. Prognostic features for breast cancer

To diagnose breast cancer using IR thermography, specific features on the surface temperature of the breasts are identified. The most common features are highly asymmetric temperature distributions between breasts, hyper thermic vascular patterns, localized hot spots, atypical complexity of the vascular pattern, temperature differences in the entire breast of more than 2 °C and areolar and peri-areolar heat patterns.

In thermography, the magnitude of the temperate gradients used to distinguish between benign and malignant tumors. High temperature gradients (>1 C) are indicators of malignant tumors and lower temperature gradients are associated with benign breast diseases.

Besides the diagnosis of breast cancer, it has been demonstrated that thermography can detect angiogenesis due to the increased demand of blood to supply the new vessels and the increased metabolic activity. Guidi and Schnitt [36] conducted an study of patients with pre-invasive breast cancer. The authors reported that women with increased number of microvessels in the breasts have up to seven times greater risk of developing breast cancer as compared with women with normal microvessel density.

Gamagami [37] conducted a clinical study on patients with breast cancer using mammography and IR thermography. He reported that hypervascularity and hyperthermia can be found in 86% of non-palpable breast cancers. The author also noted that 15% of non-palpable cancers went undetected by mammography, but detected by IR thermography.

Head et al. [38] conducted an study on 126 breast cancer deceased women, 100 living breast cancer patients and 100 healthy patients. From the group of 126 deceased women, 88% presented abnormal thermograms; from the group of 100 surviving cancer patients, 65% presented abnormal thermograms and only 28% of healthy women presented abnormal thermograms. The most relevant prognostic feature from this study is that breast cancer patients with abnormal thermograms have fast growing tumors.

Gautherie and Gross [33] conducted a clinical study on near 58,000 patients. The study took place from 1965 to 1977. From all the patients, 1527 women had thermograms stage Th III. The stages in the study range from Th I to Th V, according to an increasing probability of cancer. Each stage is identified by thermos-vascular patterns and areas of hyperthermia. In the case of Th III thermograms, these represent suspicious, but not conclusive thermograms. The study focused on patients with Th III thermograms.

Of the 1527 Th III patients, 784 had no abnormal physical, mammographic or echo graphic findings; 461 had conditions diagnosed as benign disease, mainly cystic mastopathy; and 282 had conditions confirmed as cancer. From the 784 apparently normal patients, 177 were diagnosed with cancer within the first two years after the initial examination. Additional 121 cases were

found in the next two years (4 years after the initial examination). In total, 38% of this group was diagnosed with cancer within 4 years after the initial examination. The most important observation from this study is that healthy patients with abnormal thermograms are at a higher risk of developing cancer.

Amalu [39] conducted a review of the clinical application of breast thermography for the diagnosis of breast cancer. IR thermography has a significant prognostic relevance in breast cancer because it is related to tumor growth, tumor size and the malignancy of the tumor.

2.3. Standards and operating protocols

A patient's thermogram is significantly affected by the many factors both prior to the examination and during the examination. The lack of standards and protocols was attributed to be one of the primary reasons for the poor results in the early thermography studies. Ng [22] provided a detailed account of the standards that should be followed before a patient undergoes an examination, the testing procedure and environment during the examination and the post processing of the obtained thermograms. Some of the salient points from the work are given below.

- **Patient preparation**: The food the patient consumes prior to the examination can alter the metabolic rate of the body leading to variations in the observed thermograms. Large meals, excessive consumption of beverages such as tea or coffee as well as smoking and alcohol consumption should be avoided prior to an examination. Other factors that may affect the thermogram include sunbathing- up to five days prior to the examination and application of cosmetics, lotions or antiperspirants.
- **Examination environment**: The patient should be in the examination room or a similar room 15 min prior to examination in loose fitting cloths to acclimatize to the environment. Ring [40] recommended that the examination room is 3×4 m with a carpeted floor. The room temperature should be maintained between 18 and 25 °C with a relative humidity between 40% and 75%. Heat sources such as the computers and cameras as well as heat sinks such as air conditioning ducts or water outlets should not be located near the examination area. Windows in the room must be shielded to prevent external radiation from entering the room. Low IR emitting light sources such as florescent tubes or LED lamps must be used for lighting.
- **Imaging standards:** The standards that need to be used during thermal imaging of a human subject is given by Ammer and Ring [41]. Thermal imaging cameras used to obtain the thermograms have a startup time before the images become stable. It is recommended that the camera run for at least 15 min before the start of the examination. Capture masks should be used to as references and should be 1/3 the width and 2/3 the height of the target size. The position of the camera relative to the subject should be clearly indicated if images from multiple angles are taken and the patient should not move while images from multiple angles are obtained. The detector used in the camera should have a thermal resolution of at least 100 mK at 30 °C and a special resolution of 1 mm × 1 mm. The thermograms used should have a minimum resolution of 120×120 though a higher resolution would be preferred.
- **Post processing:** The software that are used in conjunction with the thermal imaging camera should comply with a firm set of standards so that the images are not modified or the contrasts enhances in an arbitrary manner. Ring [40] proposed the standards that need to be implemented for obtaining thermograms. The algorithms used to detect hot spots or analyses the asymmetry between the beasts and identify suspect regions need to be standardized.

Typically, thermograms of three different positions are captured, one frontal and two laterals. In order to better identify the presence of a tumor and its location, thermograms of the entire breast should be obtained.

An area where medical opinion is divided is the role of artificial implants in causing cancer [42,43]. While some research has shown that silicone implants have no role in the formation of cancer, others believe that women with implants are at an increased risk of suffering from Anaplastic Large Cell Lymphoma (ALCL). In any case, developing an effective screening technique to detect breast cancer for patients with breast implants is required. Screening for breast cancer using mammography for patients with implants is not ideal as (i) it may lead to damage to the implant and (ii) the tumor may hide behind the shadow of the implant and not be detected. Using thermography for screening women with implants can be effective as the implants are normally placed at the base of the breast and do not significantly affect the heat transfer in the rest of the breast.

2.4. Image processing and automation

Lipari and Head [44] developed image processing techniques to obtain asymmetry in the heat pattern observed from high resolution thermograms. They computed the differences in temperature between the two breasts. They used uncooled IR cameras with a thermal sensitivity of 0.039 K. The thermograms were taken from the front of the breasts in order to reduce perspective and scale distortions. They segmented the breast in different quadrants to compare the differences in temperature between the contralateral breasts. They noted that the accuracy of diagnosis using IR thermography can be significantly affected due to variation in interpretation of the result by the operator. Therefore in a subsequent publication, Head et al. [45] automated the algorithm to compare the temperature profile on contralateral breasts. By comparing statistics of the entire breast with those from different quadrants of the breasts, the accuracy of the technique improved. However, from their results it is not clear how the image processing helped in the diagnosis of cancer because no significant differences in their indicators were observed between tumorous and healthy breasts. They claimed that their technique reduced the number of persons that must be screened with other techniques by determining if the abnormality level of the thermograms.

Qi and Head [46] and Kuruganti and Qi [47] proposed an automatic approach that included automatic segmentation and pattern classification of the thermograms to obtain the most relevant features. The pixel distribution is analyzed for each of the regions in the two different breasts. The procedure is able to identify abnormalities in the temperature distribution. Jakubowska et al. [48] and Wang et al. [49] studied the thermal signature of healthy breasts and those with malignant tumors. Irvine [50] explored the use of Automated Target Recognition as a possible technique to improve the diagnosis of breast cancer. In a recent publication, Borchartt et al. [51] presented a review of the advances in thermography using image processing techniques to aid in breast cancer diagnosis.

2.5. Dynamic IR thermography

Dynamic IR breast thermography is the process of capturing IR thermograms for a given time. Typically, dynamic IR thermograms are captured after subjecting the breasts to a cold stress. Usually the duration of the cold stress is short, lower than 5 min, and with temperatures ranging from 20 °C to 5 °C. Lower cooling temperatures increase the temperature contrast, i.e. the difference in temperature between the breast with a malignant tumor and the

contralateral healthy breast. However, cooler temperatures also increase the patient discomfort due to prolonged exposure of sub ambient temperatures. In most of the cases the cold stress is achieved by directing cold air to the breasts. The aim of blowing air is to reduce the temperature variations in the breasts. After applying the cold stress, IR thermograms are captured in the called recovery phase. With transient thermography, the heat patterns due to the tumor are enhanced and the tumor thermal visibility improves.

Ohashi and Uchida [52] obtained IR thermograms on 728 patients with breast cancer. The thermograms were obtained using steady state and dynamic thermography. For the steady state cases, the ambient temperature was maintained at 21 °C. In the transient cases, the thermal stress was introduced by blowing air with an electric fan during 2 min; the thermograms were captured 15 s apart during 20 min. They reported that the accuracy of breast cancer detection improved from 54% using steady state thermography to 82% using dynamic thermography.

2.5.1. Commercial diagnostic tools using dynamic IR imaging

The Sentinel BreastScan™ is a commercial Infrared system for the adjunct diagnosis of breast cancer. For the exam, the patient is disrobed from the waist up and the arms placed on an armrest. Then, cool air is directed to the breasts for 3–4 min. During the exam, the patient can see the dynamic IR thermograms on a display. Once the cool air is turned off, the exam is complete and the system will estimate the risk of breast cancer. The system determines the magnitude of the asymmetries on temperature distribution between both breasts and based on such value, generates a report with the estimation. The sensitivity of the IR camera used is 0.08 °C.

Another commercial system is the FDA cleared NoTouch BreastScan [53]. This system uses two infrared cameras with sensitivity of 0.05 °C, each directed to one breast. The breasts are cooled by 3–4 °C using air while IR thermograms are being captured. The exam takes between 5 and 6 min. The software of the NoTouch BreastScan is based on Artificial Neural Networks (ANNs). The software compares the temperature distribution with known heat patterns for cancer tumors and provides a diagnosis based on such comparisons. The technical specifications of the Sentinel BreastScan and the NoTouch BreastScan commercial products are given in Table 2.

2.5.2. Clinical studies using dynamic IR thermograms

Parisky et al. [18] captured IR transient thermograms of 875 biopsied lesions (187 malignant and 688 benign) in 769 subjects using the Sentinel BreastScan™. The IR study was conducted in one breast at a time. First one of the breasts was cooled with a flow of cold air while the other was covered; then, the procedure was repeated for the other breast. Thermograms were captured during the cooling step. Results indicated 97% sensitivity (positive diagnoses that are actually positive) and a negative predicted value of 95% (negative predictions that are actually negative). For all 875 lesions, the sensitivity and negative predicted values were better for subjects with denser breast (younger patients) tissue than for those with less dense fatty breasts. In the study conducted by Parisky et al. [18], the location of the suspected region to be biopsied was known prior the IR study. This may have biased the interpretations, leading to high prediction rates. Arora et al. [20] conducted transient IR study on 92 patients with either suspicious mammograms or ultrasound images. The authors used the Sentinel BreastScan™ system. More than 100 temperature images were captured during the cooling phase. Results indicated that 58 of the 60 malignant tumors were predicted, achieving a sensitivity of 97%. The sensitivity rate could be very high because the authors considered any slightly abnormal temperature distribution to indicate the presence of a malignant tumor.

Wishart et al. [54] used the Sentinel BreastScan™ and the NoTouch BreastScan software to analyze thermograms of 100 patients with a total of 106 biopsied tissues. 65 of the tumors were malignant and 41 benign. In their study, the sensitivity of the Sentinel BreastScan™ was 53% and that of the NoTouch BreastScan software was 70%. They included the diagnosis of a radiologist in the study, which had a sensitivity of 78%. Although the diagnosis provided by the expert radiologist was better than using the NoTouch software, the authors recognized the great improvement of the NoTouch software over previously used techniques. The authors identified the need for future research in neural network systems for breast cancer diagnosis. Collet at al. [55] used the NoTouch BreastScan system to study 99 patients for whom biopsy was recommended. There were a total of 105 biopsied tissues, 33 malignant and 72 benign. The sensitivity reported was 78.8%. They claim that this high value may be biased because the IR study was conducted after the biopsy results were disclosed.

Table 2
Comparison between the Sentinel BreastScan and the NoTouch BreastScan.

Feature	NoTouch Breast Scan	Sentinel BreastScan
Temperature sensitivity (°C)	0.05	0.08
IR camera resolution (pixel)	640 × 512	320 × 240
Number of IR cameras	2	1
Wavelength range (μm)	3.5–10.5	7–12
Transient IR	Yes	Yes
Cooling method	Cold air	Cold air
Cooling time (min)	5–6	3–4
Analysis time (min)	Immediate	4–5
Artificial intelligence	Yes	Yes

2.6. Comparison between steady state and dynamic IR thermography

Dynamic thermography increases the thermal contrast between healthy tissue and that with a malignant tumor as compared to steady state thermograms. However, the procedure still is not standardized and the cooling time and temperature are not consistent between the different studies. This may lead to the high variation in sensitivities reported between different works. Another concern in dynamic thermography is the patient discomfort due to the cooling stress, which is typically between 2 and 6 min at temperatures below 15 °C. Dynamic thermography was introduced because the sensitivity of IR detectors was lower than 50 mK and the subtle temperature variations could not be captured. With modern IR detectors, which have sensitivities higher than 20 mK, the subtle temperature variations can be accurately captured. Studies evaluating steady state thermography using high sensitive IR detectors are needed to reassess the limits of steady state thermograms and to clarify whether dynamic thermography is required or steady state thermography is capable of detecting malignant tumors.

3. Numerical simulation of cancer tumors

The interaction of tissue with nerves veins and arteries, creates a non-homogeneous complex morphology. Veins and arteries transport blood which transfers heat to the tissue. The presence of tumors, they create isolated regions with different thermal characteristics. To model tissue, scientists have proposed various mathematical models to capture the behavior of this complex material. Some of the prominent models that have been proposed are the counter current model, the dual phase lag model and the radiative model. The most commonly used bioheat equation was developed

by Pennes [56] in 1948 by observing the human forearm. It is a modified transient heat conduction equation which accounts for the metabolic heat generated within the tissue and the heat transfer between the tissue and the blood. The model assumes that heat transfer between tissue and the blood only takes place in the capillaries and not in the larger arteries/veins. The capillaries act as a heat source or heat sink depending on the ambient temperature of the tissue. In case of muscles doing work, the excess heat generated is removed by the blood whereas the capillaries act as a heat source in dormant regions like the breast. The Pennes' bioheat equation is given by,

$$\rho_t c_t \left(\frac{\partial T_t}{\partial t}\right) = \nabla \cdot (k_t \nabla T_t) + \omega_b c_b (T_a - T_t) + q_m \tag{2}$$

where ρ, c and k stand for density, heat capacity and thermal conductivity respectively. The subscripts t, b and a stand for tissue, blood and artery. The blood perfusion rate, ω is the volumetric flow rate of blood for a unit volume of tissue and q_m is the metabolic heat generation rate. The model proposed by Pennes has been extensively studied over the years and the main criticisms regarding the model are [57] – (i) combining the local effects with like heat generation, storage and diffusion with global effects such as blood perfusion and convection in a control system is not accurate, (ii) considering distinct temperatures of the tissue, blood inlet and outlet at the same point is incorrect. Various other models have been developed over the years that considered more complex formulations in order to model different phenomenon such as hypothermia. Bhowmik et al. [58] reviewed the prominent bioheat transfer models and their relevance to various applications.

The counter current model was initially proposed by Mitchell and Myers [59] and other researchers have subsequently developed variation of the model [60–63]. The model postulates that heat transfer between the body and the environment is best modeled as a cumulative effect of the counter current heat exchange process between the arteries and veins, and heat lost from the body due to convection, radiation and evaporation. The model by Mitchell and Myers was valid for sections of the body where the vessel structure was simple and the blood flow rate was low like the extremities of the body. Weinaum et al. [61,62] refined the model by classifying tissues into three categories based on the thermal interaction between the tissue and the blood vessel. The three types of tissue are: (i) deep tissue layer, (ii) intermediate layer, and (iii) cutaneous layer. While the model represents the thermal interaction between the tissue and the blood vessels well, it is inherently complex since the numerical solution to the model is obtained by solving a distinct equation for each of the tissue layers coupled by common boundary conditions between two adjacent layers.

With the advent of modern thermally driven medical procedures such as cryosurgery and treatments using lasers, bioheat models that accurately depict temperature fluctuations in the body when subjected to a pulse of heating or cooling loads have been developed. The need for a new model for such applications arises since the continuum based models (like Penne's bioheat equation and countercurrent model) assumes that a thermal disturbance instantaneously propagates throughout the domain while it has been experimentally shown that biological tissue exhibits non-Fourier like behavior (Roemer et al. [64] and Mitra et al. [65]). The duel phase lag model was developed to model highly transient systems where the Fourier's law is not valid by accounting for the phase lag as a result of the thermal inertia and microstructural interactions.

Radiation based models have also been developed to better understand the effect of irradiation on the body. Lasers pulses over a short duration have been used as a diagnostic tool as well as for certain forms of treatment such as eradication of cancerous tissue and benign tumors. Of the total intensity of laser incident on the body, a part of it gets diffused, and the rest is transmitted through the tissue collimated. As would be expected, the intensity of the collimated light reduces as the distance from the boundary where laser is incident increases. Van-Gemert [66] showed that light diffuses in the forward direction and can be estimated using a Henyey-Greenstein [67] or Legender decomposition function [68]. Therefore by using a radiation based bioheat model, the distribution of heat flux as a function of depth from the incident surface and radial distance from the incident location can be obtained.

Another important aspect of the Pennes' bioheat model is that the temperature is independent of arteriovenous structure. At the present, the effect of the location of arteries and veins on the temperature distribution of breast cancer is an unexplored field.

However, various studies provide a first insight on the thermal interaction between arteries and veins with tissue. Weinbaum and Jiji [63] indicated that the blood flow in the vessel induces a convective heat transfer. At the same time, heat travels through the vessels and tissue by conduction. The anatomical structure consists on tissue with artery and vein pairs branching. The blood flow direction is opposite in the artery and veins. The thermal interaction between vessels and tissue is more significant in the arteriovenous pairs relative to the smaller transverse arteries and veins. The authors indicated that temperature differences of vessels and tissue could be less than 0.2 °C at any location.

Other studies have shown the effect of the blood flow rates and vessel size on the temperature distribution. Chato et al. [69] theoretically analyzed heat transfer between artery and veins in a countercurrent parallel flow. Heat transfer coefficients were defined at the surface between the arteries and veins, and the blood flow varied along the axial direction. It was found that the effect of the heat transfer between arteries and veins was minimal at small vessel diameters (due to reduced heat transfer area) and at higher flow rates (superior convective heat transfer). Charny and Levin [70] analyzed the heat transfer in an arteriovenous network with nine branches that extended over the tissue. The theoretical analysis accounted for the countercurrent flow between the vessels and tissue. The tissue also transferred heat with the artery due to capillary perfusion. Also, a metabolic heat generation was included. Thermal equilibration occurred at 43 mm from the major vessels. At this distance the vessels diameters were less than 100 μm. The countercurrent heat transfer decreased the tissue temperature by 0.5 °C.

The effect of the location of artery and venous on the breast thermal behavior requires of special attention. The technical literature on breast cancer simulation lacks numerical models that account for the effect of the vessels interaction. The main challenge lies on providing a general model to capture the breast arteriovenous structure. Due to this reason, the bioheat equation proposed by Pennes is still widely used for the modeling heat transfer in the breast. In the following, a brief review on the progress in the simulation of cancer tumors will be presented.

3.1. Geometrical considerations

Different geometrical configurations have been considered as computational domains for the simulation of breast cancer tumors. These include rectangular, spherical, and geometries deformed by gravity effects. Although each of these geometries have revealed important information on the effect of the tumor on the surface temperature, still at the present the technical literature lacks a simulation that predicts the surface temperature with the actual breast shape. Simulations of cancer tumors with a more approximated breast shape could provide more accurate estimations of tumor effects on the breast thermal response.

In the following, earlier work on the various geometries used for the simulation of breast cancer is reviewed. Emphasis is put on the boundary conditions adopted by the geometries, as well as on the physical parameters of the tissue and tumor properties.

3.1.1. Rectangular domain

As a first approximation, some researchers employed rectangular domains for the simulation of breast cancer tumors. The rectangular domain uses symmetry boundary conditions on the vertical axes, which allows the flow of heat in only one direction. Under this condition, the temperature signature over the surface is directly related to the tumor size and location. Therefore, most of the works that consider rectangular geometries focus on the evaluation of predictive algorithms that use the surface temperature to determine the tumor characteristics. Das and Mishra [71] simulated breast cancer tumors in a rectangular-based shape by solving the Pennes' bioheat equation with an in-house numerical code. The computational domain and boundary conditions are shown in Fig. 4. The model neglected the different tissue layers that exist inside the breast and used homogenous properties in the tissue and tumor regions. The boundary condition at the bottom edge was a constant temperature of 32.8 °C, the top boundary had a convective heat flux condition, h = 20 W/m^2-K, which were justified with a previous numerical work [72]. The thermal properties of healthy and tumorous regions were experimentally determined [30]. Square tumors of 1.25 cm and 3.75 cm length were considered, and the breast had dimensions of 10 cm width and 5 cm height. The model estimated surface temperatures with tumors at depths of 0.25 L, 0.5 L and 0.75 L from the surface were L is the breast height. Results of the simulation were used for developing a predictive tool for the estimation of the tumor characteristics based on the surface temperature. A similar work was reported by Amri et al. [73] who considered a 3D rectangular domain with a spherical tumor. The domain had two layers, a 5 mm thick fat layer located underneath the skin surface, and a 45 mm thick gland layer located below the fat layer. The skin surface had a convective boundary condition of 13.5 W/m^2-°C which accounted for combined effects of convection, radiation and evaporation [30]. The tumor metabolic heat generation was estimated with an empirical correlation which is function of the tumor diameter [30]. Values for the metabolic rates of the various layers were taken from Ng and Sudharshan [74]. Results showed evidence of a linear relationship between the tumor depth and the length of the thermal layer at the surface. The effect of transient cooling techniques on the tumor thermal contrast was also evaluated.

The rectangular computational domain has provided a first insight on predictive models that relate the surface temperature with the tumor size and location. However, the model is not well representative of actual shape of the breast and direct comparisons with experiments have not been reported. Other shapes of the computational domain such as hemispherical have shown better approximations to experimental observations.

3.1.2. Hemispherical domain with concentric layers

Simulation of breast cancer has also used hemispherical computational domains with multiple layers that account for the non-homogenous tissue properties inside the breast. In general, it is observed that hemispherical geometries provide temperature distributions in better agreement to experimental data. Osman and Afify [75] presented the first 3-dimensional hemispherical domain for the simulation of breast cancer tumors. The domain was divided in four different concentric layers representing the deep connecting tissues (a core layer), the intermediate muscle and fat tissues (intermediate muscle and fat layers), and the underneath surface cutaneous tissues (skin and areola layer), see Fig. 5. An important consideration was a countercurrent heat exchange between the tissue and arteries, and between the tissue and veins on the intermediate layer. This effect was added to the Pennes' bioheat equation by means of extra terms with overall heat transfer coefficients per unit temperature difference between artery and tissue. The various dimensions of the layers are shown in Fig. 5. The blood perfusion was chosen based on the experimental data provided by Pennes [56] and Keller [60]. The metabolic heat generation was chosen based on experimental data [56,76,77]. At the surface an average heat transfer coefficient was chosen based on experimental data of Pennes [47]. Results showed evidence of an upper quadrant warmer than the lower quadrant due to the non-homogenous perfusion rate distribution, which is in agreement with experimental data obtained with IR camera on normal breast [78]. Osman and Afify later extended their model for the simulation of a malignant breast in which the tumor region had a metabolic heat generation and higher conductivity and perfusion rates [79]. The thermal conductivity and the metabolic heat generation of the tumor region were taken from Guatherie's experiments [30] on breast cancer tumors. The simulation found variations in surface temperature with tumors sizes in the range of 10 mm to 36 mm in diameter and depths ranging from 5 to 18 mm.

The model of Osman and Afify [75,79] demonstrated that the hemispherical domain gave results in better agreement with experimental data. Also, the temperature distribution captured the effect of the different layers in the surface temperature. However, the model made important assumptions such as concentric hemispherical layers and counter-current heat interaction between tissue and arteries, and tissue and veins. Other studies indicate that Osman and Afify's model creates non-homogenous temperature distributions with large gradients of temperature near the surface [74]. As a result, the model proposed by Osman and Afify was not greatly followed. Nevertheless, the tissue properties,

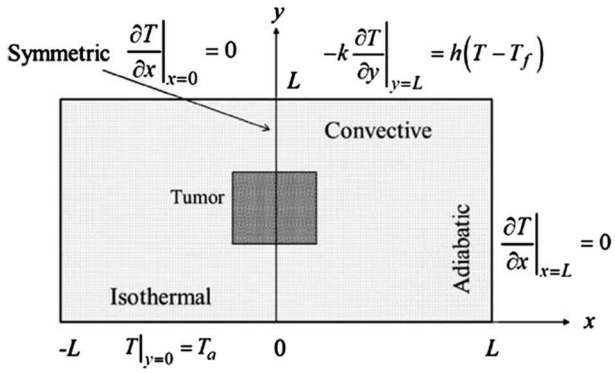

Fig. 4. Breast cancer tumor analyzed with a 2D rectangular geometry. Adapted from [71].

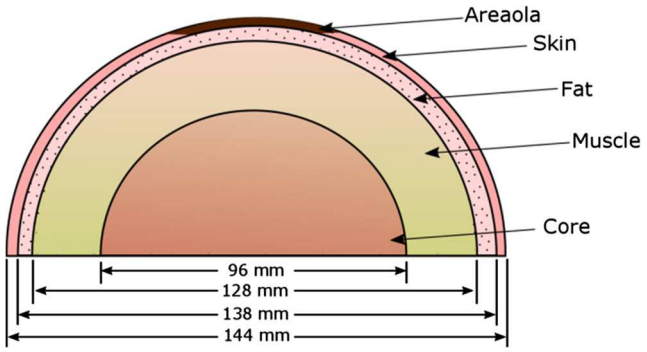

Fig. 5. Hemispherical computational domain with concentric layers. Adopted by Osman and Afify [75,79]. Redrawn from [64].

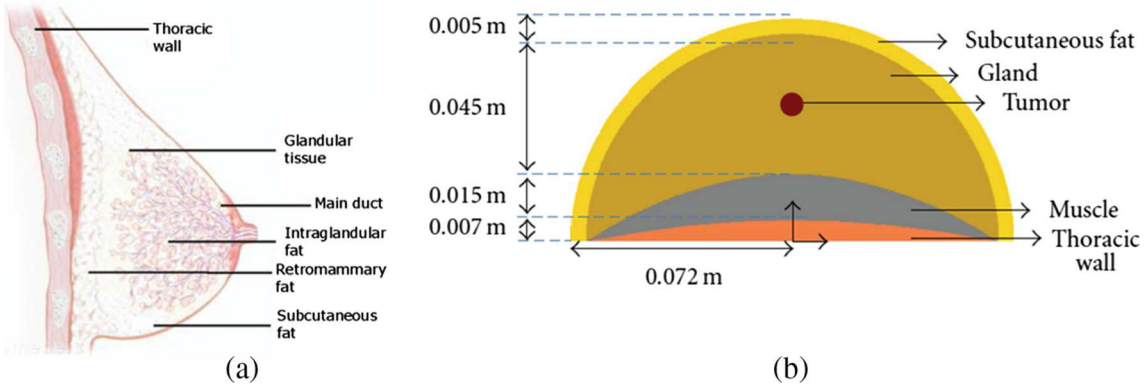

Fig. 6. Breast model in Ng and Sudharsan [74]. (a) Traditional anatomy of the breast considered by the Ng and Sudharsan with non-concentric layers. (b) Hemispherical geometry with layers of unequal proposed by Ng and Sudharsan. Adapted from [80,82].

the boundary conditions, and the hemispherical shape adopted by the authors have been commonly used in several works.

3.1.3. Hemispherical domain with non-concentric layers

The hemispherical model with concentric layers was latter modified by Ng and Sudharsan [74] to consider non-concentric layers. This configuration accounts for a gland layer occupying a larger volume inside the breast, see Fig. 6(a). The computational domain and the dimensions of the various layers are shown in Fig. 6(b). As it is shown in the figure, the breast consisted of a subcutaneous fat, a gland, a muscle and a thoracic layer. The boundary conditions were similar to Osman and Afify [75], but the governing equation was the Pennes' bioheat equation with a homogenous perfusion rate distribution and without counter-current heat interaction. The breast diameter was 23 cm, and the tumor diameters were between 10 and 30 mm. Computed results of a breast with an offset tumor showed variations of surface temperature in the range of 36–36.5 °C in agreement with Guatherie's experiments [30]. The model quantified the effect of the tumor location on the surface temperature. In a different work, Mital and Pidarati [80] used the layered model proposed by Ng and Sudharsan [74] to predict the depth, size and heat generation of a tumor based on the breast surface temperature by using numerical simulations, artificial neural networks, and genetic algorithms. Lu et al. [81] used a similar computational domain to evaluate the effect of air flows around healthy and unhealthy breast, where it was shown that the flow rate could enhance the thermal contrast.

The hemispherical domain proposed by Ng and Sudharsan [74], has been widely used in the technical literature. The main reason is the ability of reproducing surface temperatures which are in close agreement with experimental data. However, the hemispherical domain shows symmetric temperature distributions, which disagrees with previous experimental observations [78]. Osman and Affify [79] argued that the upper quadrant of the breast is warmer than the lower quadrant due to a higher vascularity. Other studies have identified non-homogeneous temperature distributions in deformed hemispherical shapes, as it will be shown in the following subsection.

3.1.4. Domains with the actual breast shape

In an attempt to get better approximations of the surface temperature, various works have virtually reconstructed the breast shape. At the present, three different approaches have been followed to reconstruct the breast: (i) tracing the outer profile of a breast mannequin with a Computer Numerical Control (CNC) machine [83], and (ii) generating a surface with Magnetic Resonance Imaging (MRI) data [84,85], and (iii) gravity deformed with an initial hemispherical domain [86]. In general, numerical models with computational domains that resemble the actual breast shape generate asymmetric surface temperatures, which is a common trend obtained with thermograms.

To develop a computational domain that is more realistic in appearance, Ng and Sudharsan [83,87] virtually reconstructed the breast of a mannequin with a 34 cup "C" brassiere size. The domain had tissue layers representing a subcutaneous fat, a gland, a core gland, a muscle, and a tumor. An embedded tumor diameter of 32 mm was considered. The thermal conductivity and metabolic rates were taken from Werner and Buse [88], and the tumor blood flow and metabolic heat were obtained from in vivo studies of Gautherie et al. [30]. Thermograms of three volunteers were selected to compare against the numerical simulation. The breast surface had an average convective heat transfer coefficient accounting for evaporation, convection, and radiation. The breast had a constant temperature in the core region, and an adiabatic condition in the subcutaneous region. Computed results showed a cold region around the nipple with a warm lower-outer quadrant and a warm upper quadrant in agreement with the thermograms.

Computational domains which resemble the actual breast have been used to track the tumor movement due to breast compression. In MRI the tumor moves when the breast is compressed between plates. This procedure increases the error in defining the tumor location. Azar et al. [84] developed a finite element model of the breast based on elastic deformations to predict the change in tumor position after a breast is compressed. The computational domain was reconstructed from MRI data by capturing axial slices of the breast. Image processing software (Scion Image and Photoshop) were used to recreate the breast surface. Three different tissue properties were considered representing fat, glandular, and cancerous tissues. Young's modulus and stress-strain properties were obtained from the experimental work of Wellman [89] on stress-strain curves on breast tissue. Errors in displacement (tracked by locating a Vitamin E marker pill over the breast surface) between the simulation and the experimental observations indicated computed errors of 0.9 mm in the x and y direction and 1.8 mm in the z direction. A similar work was reported by Abbas et al. [85] to simulate a breast compressed by two plates, were good qualitative agreement was observed against MR images of the breast of a healthy volunteer.

Jiang et al. [86,90] were the first on developing a simulation that combined the mechanical and thermal properties of the breast. The main objective was to test the effect of breast deformation by posture and gravity on the thermal behavior. A finite element method for elastic deformation was used with mechanical properties determined from [91–93]. The initial geometry was a hemisphere, which was deformed by gravity loads of various magnitudes. The computational domain had concentric skin, a fat, a sub-gland and

a core-gland layers as proposed by Osman and Affify [75]. Results indicated that the gravity deformations create an asymmetric temperature distribution with a warmer region on the upper quadrant of the breast and a colder region in bottom quadrant, see Fig. 7. This is in agreement with previous experimental observation by infrared imaging of the breast [78], which shows evidence of the feasibility of gravity-deformed breast to generate more approximated surface temperature distributions.

Simulations with computational domains with the actual breast shape have shown asymmetric temperature distributions. Asymmetric temperature distributions were observed previously by Osman and Affify while simulating a normal breast [75], but this effect was attributed to more vessels being located on the upper quadrants of the breast. Therefore, it remains unclear whether the asymmetrical temperature distributions are due to a high vascularity or to a mechanical deformation of the breast. Also, it should be mentioned that the work of Jiang et al. [86] lacks comparisons with actual breast shapes. This comparison is necessary to evaluate the accuracy of the gravity deformed model on generating the breast shapes.

3.2. Effect of the tumor size and location

The effect of the tumor size and location is a primary factor affecting the surface temperature of the breast. It is observed that such effect depends on the geometrical considerations, the boundary conditions, and the tissue properties.

Simulations with rectangular geometries have identified significant variations in the surface temperature due to the tumor location. Das and Mishra [71] simulated breast tumors by considering a square breast and tumor. The computed results indicated that tumors of 12.5 mm located at a depth of 12.5 mm and 37.5 mm raised the surface temperature 0.56 °C and 0.007 °C, respectively. The effect of the tumor size was analyzed with a tumor at the center of the domain (25 mm) which size changed from 12.5 to 37.5 mm. It was observed that the largest tumor increased the surface temperature by 0.5 °C. In a different work, Amri et al. [73] considered a 3-dimensional rectangular domain with a spherical tumor. Results showed an increase in the surface temperature in the range of 0.2–1.2 °C for tumors of 10–30 mm diameter located at less than 20 mm from the surface. For tumors located at a depth of 10 mm, a change in the tumor diameter from 10 to 30 mm increased the surface temperature by 0.2 °C. The results reported by Amri et al. indicate that the tumor depth is the dominant factor influencing the surface temperature.

The effect of the tumor location and size in domains with concentric layers has been analyzed by various researches. The results of Osman and Afify [79] showed that tumors located at a depth of 36 mm to 49.5 mm generated a surface temperature with a cold area around the tumor, which increased as the depth of the tumor decreased and as the size increased. This phenomenon was attributed to a cooling effect induced by a higher blood flow in the tumor region. Tumors located near the surface with a depth of 5 mm to 18 mm generated larger warm areas which increased as the tumor depth decreased and as the size increased. Jiang et al. [86] with a gravity-induce deformed breast showed that the tumor depth has a higher effect on the surface temperature distribution relative to the tumor diameter. As it is shown in Fig. 8, the results indicated that tumors located at 20 mm from the surface or less increased the temperature difference between normal and unhealthy breast (thermal contrast) by about 1.5 °C. On the other hand, tumor sizes of 10 to 30 mm, located at a depth of 20 mm or less, changed the thermal contrast by about 0.1 °C. Also, it was observed that tumors with a depth higher than 20 mm induced an insignificant surface temperature difference between normal and unhealthy breast.

The effect of the tumor parameters on the surface temperature with non-concentric layers has also been analyzed. Sudharsan et al. [74] found that a 15 mm tumor diameter located at 15–38 mm form the surface generated a thermal contrast of 0.6 °C and 0.01 °C, respectively. Simulations with tumors located at the center line and 15 mm below the surface indicated that tumors of 5 mm and 15 mm diameter produced surface thermal contrasts of about 0.1 °C and 0.6 °C, respectively. These results indicate that the depth of the tumor has a higher effect on the surface temperature relative to the tumor diameter. Also, it is shown that tumors located below 38 mm from the surface might not be easily detected with an IR camera. Ng and Sudharsan [94] numerically showed the formation of a warmer region on the surface above the tumor, see Fig. 9. The results identified a diameter to depth ratio of 1:3 as a possible limit for the change in surface temperature; the change in surface temperature was hardly visible with a 10 mm tumor size located at 30 mm from the surface. Lu et al. [81] found that with a flow of 1 m/s, the surface temperature difference between normal and unhealthy breast was 1.72 °C and 0.1 °C for tumors located at 2 cm and 5 cm from the surface, respectively.

The studies on the effect of location and size of the tumor show significant variations on the surface temperature. Most of the works have concluded that the tumor thermal signature over the surface is lost for tumors located at certain depth. The maximum depth that generates a thermal signature lies in the range

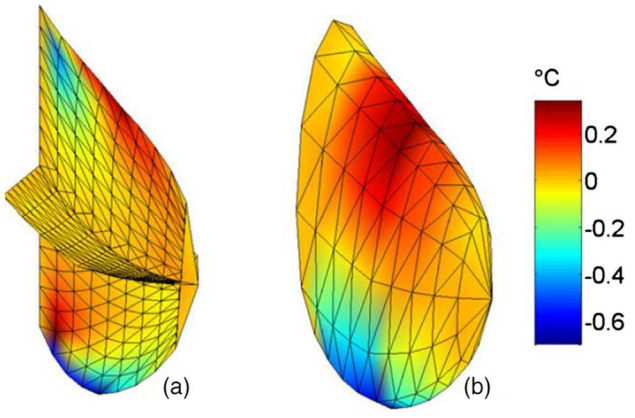

Fig. 7. Deformed spherical breast shape. Temperature difference between deformed and non-deformed breast. (a) Cross sectional temperature, (b) Surface temperature. Adapted from [90].

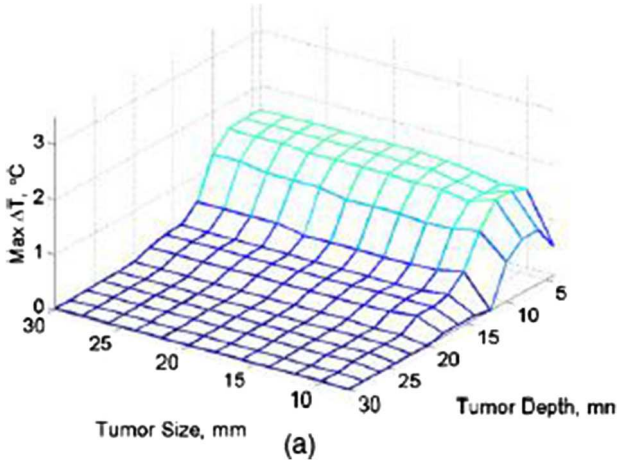

Fig. 8. Estimated maximum temperature difference between the normal and unhealthy breast. Breast deformed by gravity. Adapted from [86].

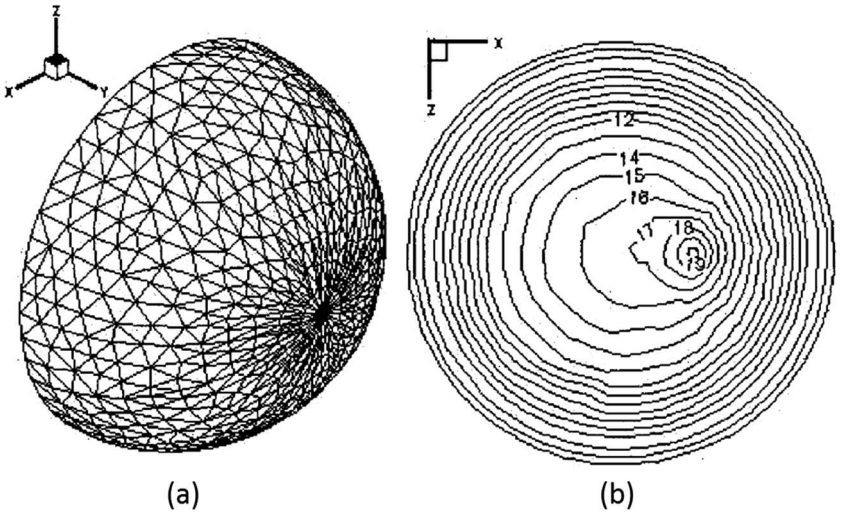

Fig. 9. Temperature distribution with an offset tumor; (a) 3D domain with the surface mesh, (b) temperature contour over the surface. Tumor size 15 mm located at 24.5 mm from the surface. Adapted from [94].

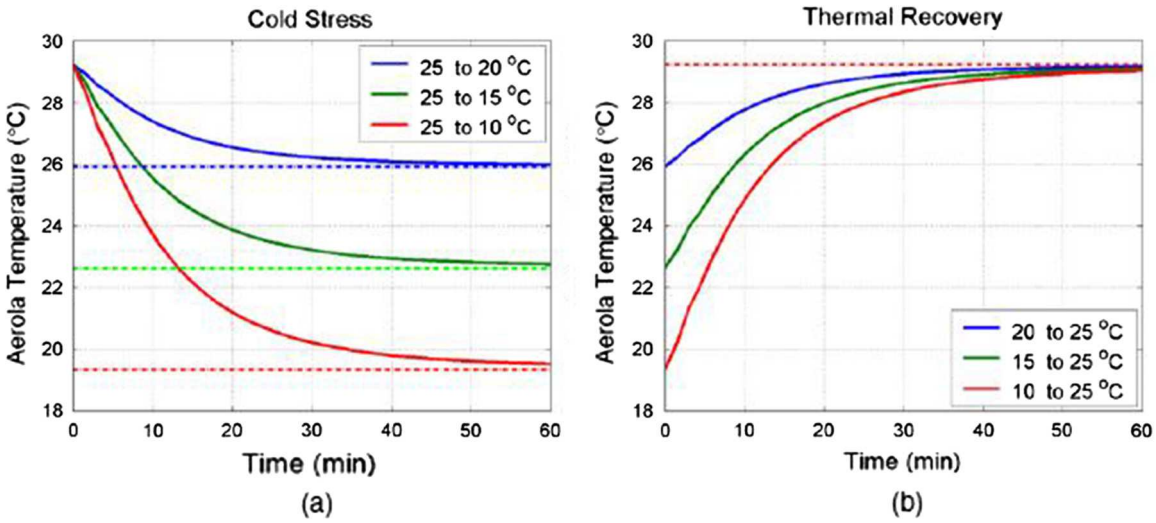

Fig. 10. Temperature at the areola as a function of time for a) cooling stress and b) thermal recovery phase. Adapted from [90].

of 20–30 mm for tumors of various diameters. Also, the surface thermal contrast increases as the tumor gets closer to the surface, maximum temperature differences between healthy and unhealthy breast of 0.6 and 1.5 °C have been identified. It has been also shown that the tumor depth has a greater effect over the surface temperature relative to the tumor diameter.

3.3. Transient numerical simulations

One of the advantages of using numerical simulations under transient breast cooling is that the effect of the cooling time and temperature on the tumor detectability can be studied without causing any discomfort on the patient. Numerical simulations allow the determination of the range of values of the cooling time and temperature that lead to higher temperature contrast between the tumor and the healthy tissue. Lower temperatures increase thermal contrast, but cause more patient discomfort. The aim of transient simulations is to find a trade-off between thermal contrast and patient discomfort to increase the detectability of malignant tumors.

Chanmugam et al. [95] studied the effects of the thermal stress on an 3D axisymmetric model of the breast. The model is similar to the model employed by Mital and Pidarati [80]. The authors compared the results of the transient simulations to a steady state case. They used COMSOL Multiphysics to perform the analysis. For the steady state case, they studied the effect of tumor size and location. For the transient simulations, they studied the effect of cooling time and cooling temperature on the surface temperature distribution during the recovery phase. They changed the temperature from 14 °C to 20 °C and the cooling time from 30 s to 120 s. They observed that the maximum temperature peak increased from 0.60 °C to 0.65 °C when the cooling time increased from 30 to 120 s. They observed that the maximum peak in temperature occurred from 0.7 to 0.9 when changing the cooling temperature from 20 °C to 14 °C.

Jiang et al. [90] compared the surface temperature distributions obtained from steady state thermograms on a breast model deformed by gravity. For the steady state case, they found temperature asymmetries on the surface temperature due to the action of gravity. They found that the surface temperature changes more by changes in depth than in changes in tumor size. The cold stress was introduced by changing the ambient temperature from its standard value at 25–20 °C, 15 °C or 10 °C. The cold stress time was varied between 0 and 60 min. They observed that the major changes in

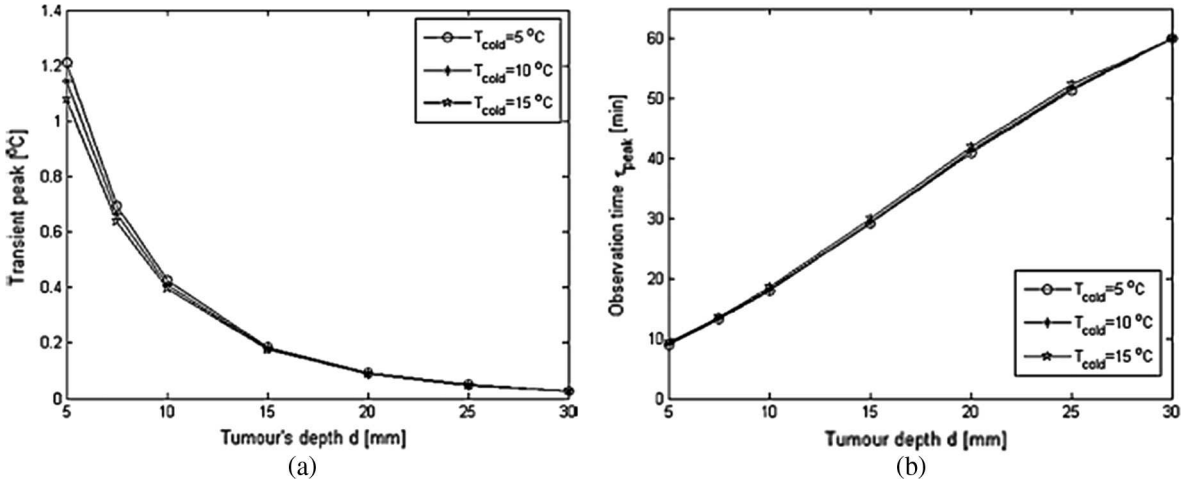

Fig. 11. Effect of cold stress temperature on a) the magnitude of the temperature contrast and b) the observation time required. Adapted from [73].

temperature occur for cold stress times lower than 10 min. After 10 min, the temperature decrease and become less steeped and finally after 30 min, the changes in temperature are very slow. Fig. 10a shows the temperature of the areola as a function of the cooling time for the different cooling temperatures considered. After removing the cold stress during the thermal recovery phase, the temperature increased considerably during the first 15 min, then, the changes were less tilted and after 25 min, the increase in temperature was very slow (Fig. 10b).

The authors noted that the maximum temperature contrast is obtained at around 30 min of the beginning of the thermal stress. However, in the real case, the patient would be subjected to a cold stress for 30 min, which can create discomfort in the patient due to the prolonged thermal stress.

In a recent work, Amri et al. [73] performed an study of steady state and transient simulations on a breast model with a malignant tumor. They used a three dimensional model consisting of a rectangular region with two different layers, the fat and the gland tissues. The depth of the model was 50 mm (5 mm fat and 45 mm gland); the tumor was embedded in the gland region. They studied the effect of the tumor diameter and depth. To study the effect of the tumor diameter, they considered diameters of 10, 20 and 30 mm. The depth of the tumor varied between 5 and 30 mm. The ambient temperature was 21 °C and the core temperature was 37 °C. For the transient simulations, the authors considered cooling temperatures of 5, 10 and 15 °C and cooling times of 10, 20, 30, 60 and 120 s. The authors compared the thermal contrast between the steady-state and transient simulations. Their results indicate that the tumor diameter has a minimal on the thermal contrast when the depth of the tumor is higher than 15 mm. They reported that the cooling temperature has little effect on the magnitude of the thermal contrast (Fig. 11a); for tumors deeper than 20 mm, the thermal contrast is as low as 0.05 °C. For example, the maximum thermal contrast for a 10 mm tumor and 1 min cooling with 5 °C located at 5 mm is obtained around 8 min with a value of 1.2 °C. They also reported that the time required to obtain the maximum thermal contrast increases as the deep of the tumor increases (Fig. 11b).

The work of Jiang et al. [90] reported cooling times of up to 1 h in order to cool the whole breast and increase the temperature contrast caused by the presence of the tumor. However, in a real case, the patient would be for 1 h subjected to a cooling stress; adopting these recommendations can cause great discomfort in the patient. In contrast, Amri et al. [73] reported optimal cooling times lower than 2 min, which is a more patient friendly approach. However, the model adopted by the authors is a rectangular domain, which does not resemble the shape of the breast. Therefore more research is needed to identify a range of cooling parameters that both, be user friendly and allow high thermal contrasts between the tumor and the healthy tissue. For tumors deeper than 15 mm, transient thermography provides similar values to steady-state thermography.

4. Inverse modeling

Inverse modeling is the estimation of the value of the unknown parameters in an equation when the solution is known. To estimate the unknown parameters, initial values are considered and the governing equation is solved for the set of estimated parameters. The estimated solution is compared with the known solution and optimization algorithms are used to estimate a new set of parameters. A new solution is then obtained for the new set of parameters. This procedure is repeated until the difference between the estimated and the known solutions be smaller than a convergence criterion. In the case of IR thermograms for breast cancer diagnosis, the surface temperature distribution obtained from IR thermograms is considered as the solution to the bio-heat transfer equation. To implement inverse modeling, a model for the breast is required. The bio-heat transfer equation is solved in such domain for a set of initial values of the thermophysical properties of the breast tissues. Then, optimization techniques such as the Gradient Descent Method, the Levenberg-Marquardt algorithm, or Genetic Algorithms are used to estimate the value of the thermophysical properties. The inverse modeling problem is typically ill posed with no unique solution since temperature can only be measured at the surface of the breast and the temperature profile inside the breast remains unknown.

4.1. Inverse modeling with analytical methods

Gescheit [96] emulated tumors by embedding paramagnetic nanoparticles in a medium. They implanted the nanoparticles at a given location and then heated the nanoparticles. An IR camera captured the surface temperature and a model based on the steady state heat equation in cylindrical coordinates was solved. They used the Levenberg-Marquardt algorithm to fit the experimental temperatures to the analytical model in order to determine the depth of the nanoparticles. The results indicated that the heat generation and depth were predicted with 0% and 4.17% variation, respectively. The conceptual work of Gescheit [96] was recently taken to the practice by Han et al. [97] who used IR camera and

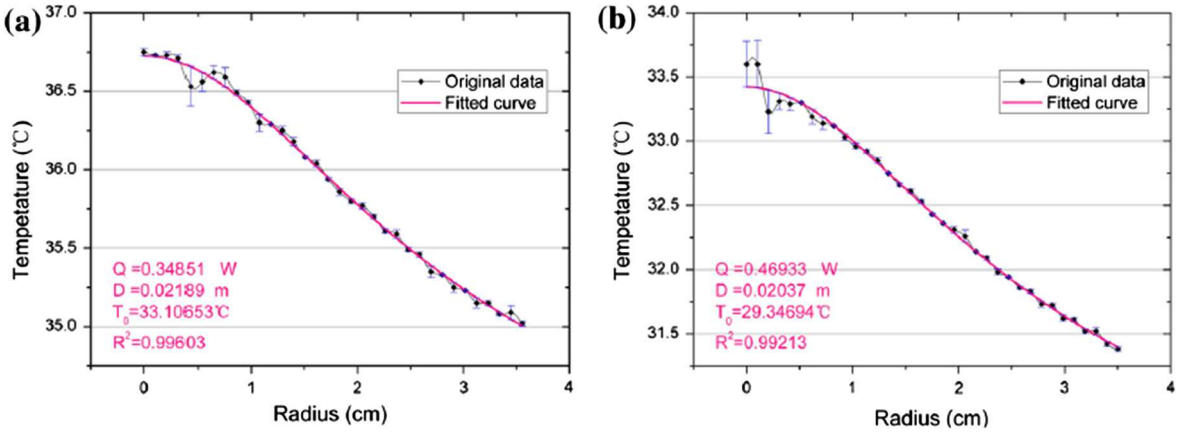

Fig. 12. Comparison of temperature distribution for the actual temperature profile and the fitted estimation (a) malignant tumor in fatty tissue and (b) malignant tumor in dense tissue. Q is the power of the source, D is the depth of the source and T_0 is the estimated basal temperature. Figure adapted from [97].

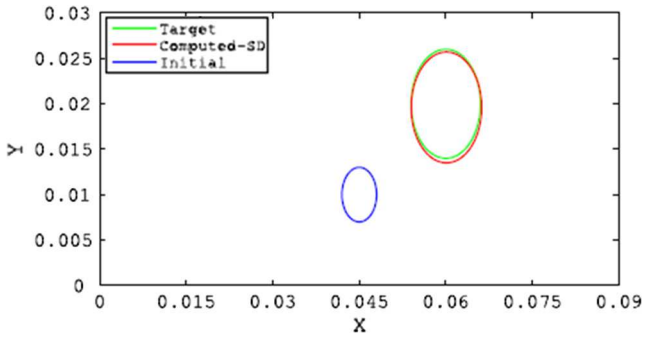

Fig. 13. Initial location of the tumor (blue), target location (green) and location predicted using the Pattern Search method (red). Figure adapted from [103]. (For interpretation of the references to colour in this figure legend, the reader is referred to the web version of this article.)

regression analysis to differentiate cancerous and benign tumors based on the tumor heat generation magnitude since cancer tumors have higher generation rates Fig. 12 shows the comparison between the experimental data and the regression analysis. Ye and Shi [98] developed a MATLAB algorithm with multiple heat sources to fit the surface temperature profile to an analytical model. They achieved a true diagnostic in 90.1% of the malignant tumors and in 83.3% of the benign tumors. The procedure was able to identify that cancer tumors are denser and with irregular shapes as compared with benign tumors.

4.2. Inverse modeling with numerical simulations

4900930182245490093043942O-1377315412115-1594485514350-1824990663575-1614805452755-1818005-82550-2021205534670-2231390643255Numerical simulations provide great insight of the thermal interactions occurring inside the breasts. Numerical simulations work well if the breast properties are provided, but because every breast is different from each other, there are not universal breast models or property values. Thermal properties of the breast vary from individual to individual and precise knowledge of the properties of the breast tissue is important to predict the presence of a tumor from a thermogram. Several authors have used numerical simulations coupled with optimization techniques to estimate the properties of the breast tissues through surface temperature readings.

Luna et al. [99] used the Boundary Element Method [100] to relate abnormal skin surface temperature with tumor position, tumor size, heat generation, and perfusion rate on a 3D rectangular domain. The authors found that their method could determine the tumor position, tumor size, and tumor heat generation within 5%, 1%, and 5% of error, respectively. Moreover, the algorithm was capable of detecting a small tumor of size 5 mm × 1 mm at a depth of 2 cm.

Paruch et al. [101] employed genetic algorithms and gradient methods to estimate thermal and geometrical parameters of breast cancer tumors. The gradient method used least square minimization to determine the unknown parameters. The results indicate that genetic algorithms identify thermal properties (power strength) with a maximum error of 0.79%. The geometrical parameters (tumor size and location) were estimated with a maximum error of 7.5%. Agnelli et al. [102] used computer simulations and evolutionary algorithms to estimate the depth, size, and thermal properties of an embedded tumor. Their method predicted tumor characteristics with more than 95% accuracy. Das and Mishra [71] estimated the location and size of the tumor from the temperature profiles of the surface using genetic algorithms. The simulations were carried out in a 2D rectangular domain and simulated using finite volume method. The location and size of the tumor is optimized till the error is minimized. Agnelli et al. [103] used pattern search algorithms to determine the metabolic heat generation and location of the tumor in a three dimensional domain. Fig. 13 shows the initial (blue) and target (green) positions of the tumor. After the algorithm was applied, the tumor position changed to the red oval, which is very close to the target position.

Jiang et al. [104] determined the properties of the breast from the thermograms of the breast surface using inverse modeling. The work is based on combined thermal and elastic modeling of a tumorous breast subjected to gravity induced deformation that has been used for the authors in other publications [86,105]. The authors reported the Tumor Induced Temperature Contrast (TITC) and reported more than 95% accuracy in the determination of thermal properties.

5. Artificial intelligence in breast cancer detection

In the context of this paper, Artificial Intelligence (AI) is a group of algorithms that can "learn" features from data. One of the most important tasks of AI is data classification. Data classification is the task of classifying previously information. To conduct data classification, the algorithm must be trained with a set of data and the corresponding classes. Support Vector Machines (SVMs) are models that incorporate supervised learning mainly for classification and regression. In SVMs, the different classes in the data are identified and the separation between classes is achieved by means

of hyperplanes. Most artificial intelligence algorithms used for breast cancer detection are classification algorithms in which the objective is to distinguish between healthy and breasts with a malignant tumor. These algorithms need to be trained with thermogram images labeled as malignant and healthy breasts.

Acharya et al. [106] used SVMs to classify 50 IR thermograms, 25 normal and 25 breasts with a cancer tumor. The authors extracted different statistical indicators such as the mean, homogeneity, energy and entropy of the thermograms. From each of the 25 thermograms in every class, the authors used 18 thermograms for training and the remaining 7 were used for testing. The use of the SVM resulted in a sensitivity of 85.71% and a specificity of 90.48%. The sensitivity is higher than the typical sensitivity achieved by an expert radiologist, which is around 78%. The results obtained by the authors are promising, but the database that they used for training and test was very small. Therefore, the results cannot be generalized. Tan et al. [107] collected 6000 temperature sets obtained from 16 thermocouples placed on the breasts of patients; 16 thermocouples per patient, 8 on each breast. They used different 5 different classifiers, named feed forward neural network, probabilistic neural network, fuzzy classifier, and Gaussian mixture model and support vector machine. They used 5000 data for training and 1000 data for testing the classifiers. All classifiers achieved specificities above 80%. The best performance was achieved by the SVM, with an average precision of 90.4%. Recently, Francis et al. [108] used a SVM to classify abnormal thermograms with an accuracy of 90.91%.

5.1. Artificial Neural Networks (ANNs)

Artificial Neural Networks (ANN) are algorithms trained with data which purpose is to make predictions. In a neural network, data is fed to the input layer and then processed in the hidden layers. Finally, the output from the last hidden layer serves as input to the neurons in the output layer and a decision is taken. There could be as many hidden layers as desired as well as neurons per layer. ANNs have been widely used in problems related with classification and recognition of objects within an image, achieving high prediction rates. Recently, ANNs have been used to predict the presence of breast cancer given a thermogram. To train the ANN, many images both with cancer and without breast cancer must be provided to the algorithm.

Ng and Kee [78] used ANNs and bio-statistical methods to detect cancerous tumors from IR thermograms. The thermograms of 82 patients (30 asymptomatic, 48 benign and 4 malignant) were used in the analysis. The inputs of the ANN were determined from a regression analysis. To train their ANN, the authors used a radial basis function with back propagation. The outputs were positive (1) for malignant and benign cases or negative (0) for healthy cases. The authors reported a maximum accuracy of 80.95% in detecting the tumor. The radial basis function had 75% accuracy in making a true diagnostic in the unhealthy population, and 90% accuracy in the healthy population.

Mital and Pidarati [80], combined ANNs, genetic algorithms, and computer simulations to relate the skin surface temperature with the tumor depth, diameter, and heat generation. The ANN was trained with the tumor characteristics to predict the surface temperature distribution. A genetic algorithm received an experimental or numerical temperature to find the corresponding tumor parameters with an initial population conformed by the outputs of the neural network. The computational domain consisted of a layered semi-spherical breast (Fig. 14a)). The surface temperatures found with the ANN showed good agreement with the numerical simulation (Fig. 14c)). The genetic algorithm determined tumor depth and diameter within an error of 5 mm and 2 mm, respectively.

In general, predictions using IR thermograms [78] present more error than predictions using numerical simulations [80,99]. This is because the thermophysical properties in the numerical simulations are considered isotropic and surface temperature variations are due only to changes in factors such as metabolic rate, tumor depth and position and not due to local changes in the structure of the breast. One of the benefits of using computers simulations to train the ANNs is that the number of cases available is not limited to the amount of clinical data since changing tumor parameters leads to a new training data. However, the numerical model employed must be well validated with clinical data in order to produce accurate surface temperatures.

6. Current status and future research needs

6.1. Numerical simulations with more realistic computational domains

Simulations rely on governing equations that are numerically solved based on the conditions applied along the boundaries of the domain and the properties of the various tissue layers. There-

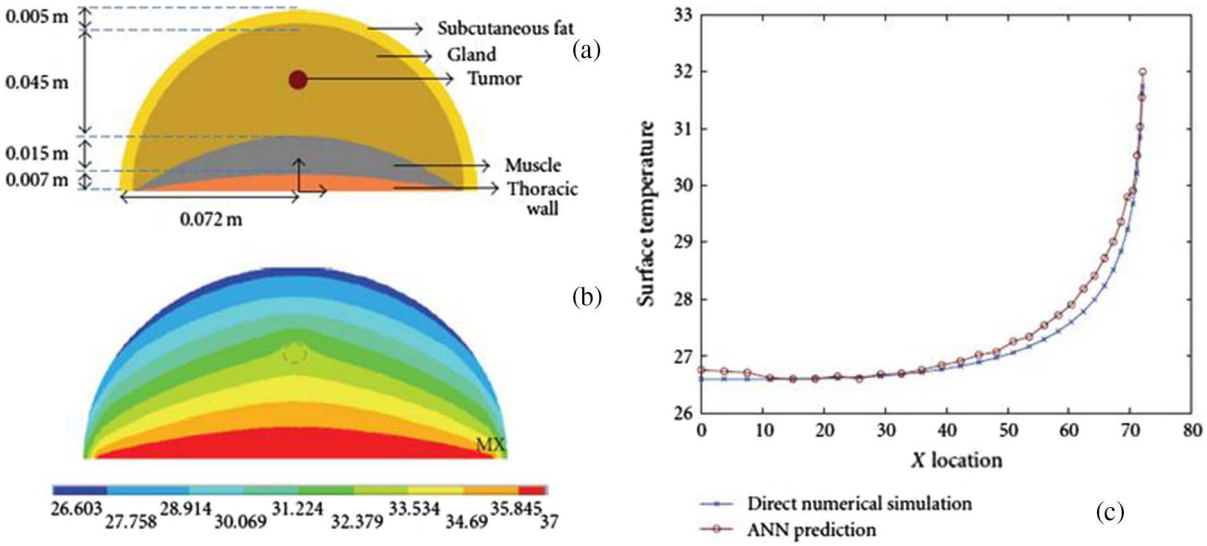

Fig. 14. (a) 2D breast model used by [80], (b) temperature distribution in the computational domain, and (c) comparison of surface temperature from the direct simulations and ANN. Figure adapted from [80].

fore, the form of the computational domain is one of the most important factors to be considered while performing a simulation. The computational domains have evolved from rectangular to the actual breast geometry reconstructed from MRI. Rectangular domains have provided a first insight into the procedures needed to use numerical methods and artificial intelligence to predict the tumor characteristics (location, size, heat generation, etc.). These analyses have also provided information regarding tumor displacement due to breast deformation. However, it is recommended that future numerical simulations should obtain surface temperature distribution using 3D reconstructed breast geometries. Jiang et al. [86] presented the first thermal-elastic model to investigate the effect of gravity deformation on the surface temperature, but the computational domain was generated by applying a gravity load to an initial hemispherical domain, and the generated geometry was not validated with the actual shape. The solution of the bioheat equation in the actual shape of the breast will be able to predict the surface temperature profile more accurately. This level of accuracy is critical to reveal the exact relationship between the tumor characteristics and its thermal signature.

6.2. Validation of numerical simulations

Numerical simulations have highlighted the most important effects of the tumor on the breast thermal profile. Such numerical models use thermal and mechanical properties for the healthy and unhealthy regions, which have been experimentally determined. However, a numerical model can only be improved by comparing the computed results against experimental data. Future research should consider the development of models that reproduce all the common thermal trends observed over the breast surface. The simulations in Ng and Sudharsan [74,94] showed surface temperatures which are in close agreement with experimental values, but their model generated homogeneous temperature distributions which is not in accordance with previously reported IR images [78]. The model of Osman and Affify [75,79] with concentric layers has asymmetric temperature distributions and colder temperatures around the areola region, but it considered arteriovenous heat exchange which has been proven to be a non-valid assumption for the breast [74]. The gravity deformed model proposed by Jiang et al. [86] showed asymmetric temperature distributions, but the areola region was not colder, as has been observed with the IR images [78]. Therefore, future advances are needed on developing an improved model that resembles the thermal characteristics of the breast with and without a tumor. Such a model is needed to more accurately determine the variations in the surface temperature due to the existence of a cancerous tumor. Moreover, this model will contribute on establishing the changes in the thermal contrast when the breast is subjected to transient cooling techniques.

6.3. Accuracy

The low sensitivity of IR detectors and the lack of standardized acquisition procedures have been the two major limitations for high accuracy in the diagnosis of breast cancer. The sensitivity of IR cameras has improved from 0.5 °C in the 1960 decade to below 0.02 °C in modern IR cameras. With modern IR cameras, it is possible to capture accurately the more subtle temperature variations in the breasts. In regards to the acquisition procedure, conditions such as the ambient and the imaging position of the patient were not regulated until recently. Nowadays, there exists a protocol for IR breast thermography in order to improve the quality of thermograms and to remove undesired effects such as cooling due to evaporation of sweat.

The accuracy in breast cancer detection has increased with the improvement of IR detectors and imaging conditions. Recent studies report typical accuracies of 78% (Wishart et al. [54]) using IR detectors with a sensibility of 0.08 °C. Further research is needed to investigate the effect of using IR detectors with sensitivities below 0.02 °C on the accuracy detection of breast cancer.

6.4. Patient discomfort

One of the most important aspects in the diagnosis of breast cancer is the patient comfort during the procedure. In the case of transient thermograms, these have shown higher contrast between the tumor and the healthy breast as compared with steady-state thermograms. However this increase in contrast is significant only when the tumor is shallow, at depths less than 15 mm. To induce the higher contrast, cold air typically between 5 °C and 15 °C is blown to the breasts for periods of time between 2 min and 6 min. The maximum contrast is achieved with colder air directed for longer periods of time. However, these conditions result in more discomfort to the patient. The numerical simulations of Amri et al. [73] show that the maximum contrast caused by a malignant tumor 15 mm deep is 0.2 °C when cooled for 2 min with air at 10 °C; the observation time required to obtain this maximum contrast is 30 min. For deep tumors, the contrast obtained using transient thermography is similar to the contrast obtained using steady-state thermograms. The advantage of steady state over transient thermography is that it does not cause patient discomfort due to an exposure to a cold air stream.In conclusion, breast cancer is a significant cause of morbidity and mortality worldwide. Early detection and secondary prevention of advanced disease remains the most effective means of reducing the impact of this potentially lethal disease. Current methods of screening are effective but inadequate; innovative methods to detect early breast cancer efficiently and without excessive discomfort are needed to improve the current state. Thermal analysis seems to be an effective way to develop this non-ordinary tool. Over the last decade, significant advances have been made in various areas, which could potentially apply this technology more effectively. IR cameras are now capable of detecting temperature variations of 0.02 K or less. Protocols to detect cancerous tumors are now standardized. Mathematical models have been developed to relate the surface temperature with the tissue and tumor properties which show good agreement with experimental data. Computer software can now virtually reconstruct the anatomy of the breast with MRI scans. Artificial intelligence has proved to be an effective tool to classify the tumor with high specificity and sensitivity values. Unfortunately, these areas are not yet linked, and effort is needed on combining these multidisciplinary advancements. The energy and faith that we dedicate to this endeavor will lead to a more effective, less expensive and more comfortable tool for reducing the health impact of this common malady.

Acknowledgement

The authors gratefully acknowledge the financial support from National Science Foundation under Contract No. CBET-1640309.

References

[1] R. Doll, R. Peto, The causes of cancer: quantitative estimates of avoidable risks of cancer in the United States today, J. Natl. Cancer Inst. 66 (6) (1981) 1192–1308.
[2] B.N. Ames, L.S. Gold, W.C. Willett, The causes and prevention of cancer, Proc. Natl. Acad. Sci. 92 (12) (1995) 5258–5265.
[3] American Cancer Society, Cancer Treatment & Survivorship Facts & Figures, American Cancer Society, 2014.
[4] American Cancer Society, Cancer Facts & Figures 2014, American Cancer Society, 2014.

[5] A.B. Mariotto, K. Robin Yabroff, Y. Shao, E.J. Feuer, M.L. Brown, Projections of the cost of cancer care in the United States: 2010–2020, JNCI J. Natl. Cancer Inst. 103 (2) (2011) 117–128.
[6] R.L. Siegel, K.D. Miller, A. Jemal, Cancer statistics, 2016, CA. Cancer J. Clin. 66 (1) (2016) 7–30.
[7] L. Tabár et al., Reduction in mortality from breast cancer after mass screening with mammography, The Lancet 325 (8433) (1985) 829–832.
[8] J.G. Elmore, M.B. Barton, V.M. Moceri, S. Polk, P.J. Arena, S.W. Fletcher, Ten-year risk of false positive screening mammograms and clinical breast examinations, N. Engl. J. Med. 338 (16) (1998) 1089–1096.
[9] K. Kerlikowske, D. Grady, J. Barclay, E. Sickles, V. Ernster, Effect of age, breast density, and family history on the sensitivity of first screening mammography, JAMA 276 (1) (1996).
[10] D. Saslow et al., American cancer society guidelines for breast screening with MRI as an adjunct to mammography, CA. Cancer J. Clin. 57 (2) (2007) 75–89.
[11] E. Warner et al., Surveillance of BRCA1 and BRCA2 mutation carriers with magnetic resonance imaging, ultrasound, mammography, and clinical breast examination, JAMA 292 (11) (2004) 1317–1325.
[12] E.A. Morris et al., MRI of occult breast carcinoma in a high-risk population, Am. J. Roentgenol. 181 (3) (2003) 619–626.
[13] W.A. Berg et al., Combined screening with ultrasound and mammography compared to mammography alone in women at elevated risk of breast cancer: results of the first-year screen in ACRIN 6666, JAMA J. Am. Med. Assoc. 299 (18) (2008) 2151–2163.
[14] S.M. Friedewald et al., Breast cancer screening using tomosynthesis in combination with digital mammography, JAMA 311 (24) (2014) 2499.
[15] T.J. Hall, Y. Zhu, C.S. Spalding, In vivo real-time freehand palpation imaging, Ultrasound Med. Biol. 29 (3) (2003) 427–435.
[16] T. Yahara, T. Koga, S. Yoshida, S. Nakagawa, H. Deguchi, and K. Shirouzu, Relationship Between Microvessel Density and Thermographic Hot Areas in Breast Cancer, Surg. Today, vol. 33, no. 4, pp. 243–248.
[17] T.D. Vreugdenburg, C.D. Willis, L. Mundy, J.E. Hiller, A systematic review of elastography, electrical impedance scanning, and digital infrared thermography for breast cancer screening and diagnosis, Breast Cancer Res. Treat. 137 (3) (2013) 665–676.
[18] Y.R. Parisky et al., Efficacy of computerized infrared imaging analysis to evaluate mammographically suspicious lesions, Am. J. Roentgenol. 180 (1) (2003) 263–269.
[19] X. Tang, H. Ding, Y. Yuan, Q. Wang, Morphological measurement of localized temperature increase amplitudes in breast infrared thermograms and its clinical application, Biomed. Signal Process. Control 3 (4) (2008) 312–318.
[20] N. Arora et al., Effectiveness of a noninvasive digital infrared thermal imaging system in the detection of breast cancer, Am. J. Surg. 196 (4) (2008) 523–526.
[21] M. Kontos, R. Wilson, I. Fentiman, Digital infrared thermal imaging (DITI) of breast lesions: sensitivity and specificity of detection of primary breast cancers, Clin. Radiol. 66 (6) (2011) 536–539.
[22] E.Y.-K. Ng, A review of thermography as promising non-invasive detection modality for breast tumor, Int. J. Therm. Sci. 48 (5) (2009) 849–859.
[23] J.D. Hardy, The radiation of heat from the human body, J. Clin. Invest. 13 (4) (1934) 615–620.
[24] D.J. Watmough, R. Oliver, Wavelength dependence of skin emissivity, Phys. Med. Biol. 14 (2) (1969) 201.
[25] J. Steketee, Spectral emissivity of skin and pericardium, Phys. Med. Biol. 18 (5) (1973) 686.
[26] K.D. Patil, J.R. Williams, K.L. Williams, Thermographic localization of incompetent perforating veins in the leg, Br. Med. J. 1 (5690) (1970) 195–197.
[27] R. Lawson, Implications of surface temperatures in the diagnosis of breast cancer, Can. Med. Assoc. J. 75 (4) (1956) 309–310.
[28] R.N. Lawson, M.S. Chughtai, Breast cancer and body temperature, Can. Med. Assoc. J. 88 (2) (1963) 68–70.
[29] T.W. Davison, K.L. Ewing, J. Fergason, M. Chapman, A. Can, C.C. Voorhis, Detection of breast cancer by liquid crystal thermography. A preliminary report, Cancer 29 (5) (1972) 1123–1132.
[30] M. Gautherie, Thermopathology of breast cancer: measurement and analysis of in vivo temperature and blood flow, Ann. N. Y. Acad. Sci. 335 (1) (Mar. 1980) 383–415.
[31] M. Kaczmarek, A. Nowakowski, Analysis of transient thermal processes for improved visualization of breast cancer using IR imaging, Proceedings of the 25th Annual International Conference of the IEEE Engineering in Medicine and Biology Society, vol. 2, 2003, pp. 1113–1116.
[32] M. Gautherie, Thermobiological assessment of benign and malignant breast diseases, Am. J. Obstet. Gynecol. 147 (8) (1983) 861–869.
[33] M. Gautherie, C.M. Gros, Breast thermography and cancer risk prediction, Cancer 45 (1) (1980) 51–56.
[34] D.A. Kennedy, T. Lee, D. Seely, A comparative review of thermography as a breast cancer screening technique, Integr. Cancer Ther. 8 (1) (2009) 9–16.
[35] J.R. Keyserlingk, P.D. Ahlgren, E. Yu, N. Belliveau, M. Yassa, Functional infrared imaging of the breast, IEEE Eng. Med. Biol. Mag. 19 (3) (2000) 30–41.
[36] A.J. Guidi, S.J. Schnitt, Angiogenesis in preinvasive lesions of the breast, Breast J. 2 (6) (1996) 364–369.
[37] P. Gamagami, Indirect Signs of Breast Cancer: Angiogenesis Study, Atlas Mammogr, 1996.
[38] J.F. Head, F. Wang, R.L. Elliott, Breast thermography is a noninvasive prognostic procedure that predicts tumor growth rate in breast cancer patients, Ann. N. Y. Acad. Sci. 698 (1) (1993) 153–158.
[39] W.C. Amalu, A review of breast thermography, Int. Acad. Clini. Thermol. (2003).
[40] E.F. Ring, Quantitative thermal imaging, Clin. Phys. Physiol. Meas. Off. J. Hosp. Phys. Assoc. Dtsch. Ges. Für Med. Phys. Eur. Fed. Organ. Med. Phys. 11 (Suppl A) (1990) 87–95.
[41] Kurt Ammer, Francis J. Ring, Standard procedures for infrared imaging in medicine, in: Medical Infrared Imaging, CRC Press, 2012, pp. 1–14.
[42] D. de Jong, W.E. Vasmel, J. Paul de Boer, et al., Anaplastic large-cell lymphoma in women with breast implants, JAMA 300 (17) (2008) 2030–2035.
[43] S. Bondurant, V. Ernster, and R. Herdman, Silicone Breast Implants and Cancer, 1999.
[44] C.A. Lipari, J.F. Head, Advanced infrared image processing for breast cancer risk assessment, Proceedings of the 19th Annual International Conference of the IEEE Engineering in Medicine and Biology Society, vol. 2, 1997, pp. 673–676.
[45] J.F. Head, C.A. Lipari, R.L. Elliot, Computerized image analysis of digitized infrared images of breasts from a scanning infrared imaging system, 1998, vol. 3436, pp. 290–294.
[46] H. Qi, J.F. Head, Asymmetry analysis using automatic segmentation and classification for breast cancer detection in thermograms, Proceedings of the 23rd Annual International Conference of the IEEE Engineering in Medicine and Biology Society, vol. 3, 2001, pp. 2866–2869.
[47] P.T. Kuruganti, H. Qi, Asymmetry analysis in breast cancer detection using thermal infrared images, Engineering in Medicine and Biology, 2002. 24th Annual Conference and the Annual Fall Meeting of the Biomedical Engineering Society EMBS/BMES Conference, 2002. Proceedings of the Second Joint, vol. 2, 2002, pp. 1155–1156.
[48] T. Jakubowska, B. Wiecek, M. Wysocki, C. Drews-Peszynski, Thermal signatures for breast cancer screening comparative study, Proceedings of the 25th Annual International Conference of the IEEE Engineering in Medicine and Biology Society, vol. 2, 2003, pp. 1117–1120.
[49] J. Wang et al., Evaluation of the diagnostic performance of infrared imaging of the breast: a preliminary study, Biomed. Eng. Online 9 (2010) 3.
[50] J.M. Irvine, Targeting breast cancer detection with military technology, IEEE Eng. Med. Biol. Mag. 21 (6) (2002) 36–40.
[51] T.B. Borchartt, A. Conci, R.C.F. Lima, R. Resmini, A. Sanchez, Breast thermography from an image processing viewpoint: a survey, Signal Process. 93 (10) (2013) 2785–2803.
[52] Y. Ohashi, I. Uchida, Applying dynamic thermography in the diagnosis of breast cancer, IEEE Eng. Med. Biol. Mag. 19 (3) (2000) 42–51.
[53] NoTouch BreastScan. Available: <http://www.notouchbreastscan.com/> [Accessed: 17-Sep-2016].
[54] G.C. Wishart et al., The accuracy of digital infrared imaging for breast cancer detection in women undergoing breast biopsy, Eur. J. Surg. Oncol. EJSO 36 (6) (2010) 535–540.
[55] A.E. Collett, C. Guilfoyle, E.J. Gracely, T.G. Frazier, A.V. Barrio, Infrared imaging does not predict the presence of malignancy in patients with suspicious radiologic breast abnormalities, Breast J. 20 (4) (2014) 375–380.
[56] H.H. Pennes, Analysis of tissue and arterial blood temperatures in the resting human forearm, J. Appl. Physiol. 85 (1) (1998) 5–34.
[57] W. Wulff, The energy conservation equation for living tissue, IEEE Trans. Biomed. Eng. BME-21 (6) (1974) 494–495.
[58] A. Bhowmik, R. Singh, R. Repaka, S.C. Mishra, Conventional and newly developed bioheat transport models in vascularized tissues: a review, J. Therm. Biol. 38 (3) (2013) 107–125.
[59] J.W. Mitchell, G.E. Myers, An analytical model of the counter-current heat exchange phenomena, Biophys. J. 8 (8) (1968) 897–911.
[60] K.H. Keller, L. Seiler, An analysis of peripheral heat transfer in man, J. Appl. Physiol. 30 (5) (1971) 779–786.
[61] S. Weinbaum, L.M. Jiji, D.E. Lemons, Theory and experiment for the effect of vascular microstructure on surface tissue heat transfer–Part I: Anatomical foundation and model conceptualization, J. Biomech. Eng. 106 (4) (1984) 321–330.
[62] L.M. Jiji, S. Weinbaum, D.E. Lemons, Theory and experiment for the effect of vascular microstructure on surface tissue heat transfer–Part II: Model formulation and solution, J. Biomech. Eng. 106 (4) (1984) 331–341.
[63] S. Weinbaum, L.M. Jiji, A new simplified bioheat equation for the effect of blood flow on local average tissue temperature, J. Biomech. Eng. 107 (2) (1985) 131–139.
[64] R.B. Roemer, J.R. Oleson, T.C. Cetas, Oscillatory temperature response to constant power applied to canine muscle, Am. J. Physiol. 249 (2 Pt 2) (1985) R153–R158.
[65] K. Mitra, S. Kumar, A. Vedevarz, M.K. Moallemi, Experimental evidence of hyperbolic heat conduction in processed meat, J. Heat Transf. 117 (3) (1995) 568–573.
[66] M.J. van Gemert, S.L. Jacques, H.J. Sterenborg, W.M. Star, Skin optics, IEEE Trans. Biomed. Eng. 36 (12) (1989) 1146–1154.
[67] L.G. Henyey, J.L. Greenstein, Diffuse radiation in the Galaxy, Astrophys. J. 93 (1941) 70–83.
[68] M.F. Modest, Chapter 12 - radiative properties of semitransparent media, in Radiative Heat Transfer, second ed., Academic Press, Burlington, 2003, pp. 413–422.
[69] J. Chato, Heat-transfer to blood-vessels, J. Biomech. Eng.-Trans. ASME 102 (2) (1980) 110–118.
[70] C. Charny, R. Levin, Bioheat transfer in a branching countercurrent network during hyperthermia, J. Biomech. Eng.-Trans. Asme. 111 (4) (1989) 263–270.

[71] K. Das, S.C. Mishra, Estimation of tumor characteristics in a breast tissue with known skin surface temperature, J. Therm. Biol. 38 (6) (2013) 311–317.
[72] H. Zhang, Lattice Boltzmann method for solving the bioheat equation, Phys. Med. Biol. 53 (3) (2008) N15.
[73] A. Amri, S.H. Pulko, A.J. Wilkinson, Potentialities of steady-state and transient thermography in breast tumour depth detection: a numerical study, Comput. Methods Programs Biomed. 123 (2016) 68–80.
[74] N.M. Sudharsan, E.Y.K. Ng, S.L. Teh, Surface temperature distribution of a breast with and without tumour, Comput. Methods Biomech. Biomed. Engin. 2 (3) (1999) 187–199.
[75] M.M. Osman, E.M. Afify, Thermal modeling of the normal woman's breast, J. Biomech. Eng. 106 (2) (1984) 123–130.
[76] E.H. Wissler, Steady-state temperature distribution in man, J. Appl. Physiol. 16 (4) (1961) 734–740.
[77] J.C.H. Chato, Thermal behavior of biological media, 01-Jun-1970.
[78] E.Y.K. Ng, E.C. Kee, Advanced integrated technique in breast cancer thermography, J. Med. Eng. Technol. 32 (2) (2008) 103–114.
[79] M.M. Osman, E.M. Afify, Thermal modeling of the malignant woman's breast, J. Biomech. Eng. 110 (4) (1988) 269–276.
[80] M. Mital, R.M. Pidaparti, Breast tumor simulation and parameters estimation using evolutionary algorithms, Model Simul. Eng. (2008), pp. 4:1–4:6.
[81] L. Hu, A. Gupta, J.P. Gore, L.X. Xu, Effect of forced convection on the skin thermal expression of breast cancer, J. Biomech. Eng. 126 (2) (2004) 204–211.
[82] D.T. Geddes, Inside the lactating breast: the latest anatomy research, J. Midwifery Women's Health 52 (6) (2007) 556–563.
[83] E.Y.K. Ng, N.M. Sudharsan, Numerical computation as a tool to aid thermographic interpretation, J. Med. Eng. Technol. 25 (2) (2001) 53–60.
[84] F.S. Azar, D.N. Metaxas, M.D. Schnall, A finite element model of the breast for predicting mechanical deformations during biopsy procedures. In: IEEE Workshop on Mathematical Methods in Biomedical Image Analysis, 2000. Proceedings, 2000, pp. 38–45.
[85] A. Samani, J. Bishop, M.J. Yaffe, D.B. Plewes, Biomechanical 3-D finite element modeling of the human breast using MRI data, IEEE Trans. Med. Imag. 20 (4) (2001) 271–279.
[86] L. Jiang, W. Zhan, M. Loew, Combined thermal and elastic modeling of the normal and tumorous breast, 2008, p. 69161E.
[87] E.-K. Ng, N.M. Sudharsan, Effect of blood flow, tumour and cold stress in a female breast: a novel time-accurate computer simulation, Proc. Inst. Mech. Eng. [H] 215 (4) (2001) 393–404.
[88] J. Werner, M. Buse, Temperature profiles with respect to inhomogeneity and geometry of the human body, J. Appl. Physiol. 65 (3) (1988) 1110–1118.
[89] P.S. Wellman, R.D. Howe, Modeling probe and tissue interaction for tumor feature extraction, in: ASME Summer Bioengineering Conference, Sun River, Oregon 35 (1997) 237.
[90] L. Jiang, W. Zhan, M.H. Loew, Modeling static and dynamic thermography of the human breast under elastic deformation, Phys. Med. Biol. 56 (1) (2011) 187.
[91] L.S. Wilson, D.E. Robinson, M.J. Dadd, Elastography - the movement begins, Phys. Med. Biol. 45 (6) (2000) 1409.
[92] S.A. Kruse et al., Tissue characterization using magnetic resonance elastography: preliminary results, Phys. Med. Biol. 45 (6) (2000) 1579.
[93] R. Sinkus, J. Lorenzen, D. Schrader, M. Lorenzen, M. Dargatz, D. Holz, High-resolution tensor MR elastography for breast tumour detection, Phys. Med. Biol. 45 (6) (2000) 1649.
[94] E.Y.K. Ng, N.M. Sudharsan, An improved three-dimensional direct numerical modelling and thermal analysis of a female breast with tumour, Proc. Inst. Mech. Eng. [H] 215 (1) (2001) 25–37.
[95] A. Chanmugam, R. Hatwar, C. Herman, Thermal analysis of cancerous breast model, presented at the IMECE.
[96] I.M. Gescheit, A. Dayan, M. Ben-David, I. Gannot, Minimal-invasive thermal imaging of a malignant tumor: a simple model and algorithm, Med. Phys. 37 (1) (2010) 211–216.
[97] F. Han, G. Shi, C. Liang, L. Wang, K. Li, A simple and efficient method for breast cancer diagnosis based on infrared thermal imaging, Cell Biochem. Biophys. 71 (1) (2014) 491–498.
[98] F. Ye, G.L. Shi, Clinical breast cancer analysis with surface fitting in the medical thermal texture maps, Appl. Mech. Mater. 263–266 (2012) 2454–2457.
[99] J. Manuel Luna, R. Romero-Mendez, A. Hernandez-Guerrero, F. Elizalde-Blancas, Procedure to estimate thermophysical and geometrical parameters of embedded cancerous lesions using thermography, J. Biomech. Eng. 134(3) (2012) 031008–031008.
[100] J.T. Katsikadelis, Boundary Elements: Theory and Applications, Elsevier, 2002.
[101] M. Paruch, E. Majchrzak, Identification of tumor region parameters using evolutionary algorithm and multiple reciprocity boundary element method, Eng. Appl. Artif. Intell. 20 (5) (2007) 647–655.
[102] J.P. Agnelli, A.A. Barrea, C.V. Turner, Tumor location and parameter estimation by thermography, Math. Comput. Model. 53 (7–8) (2011) 1527–1534.
[103] J.P. Agnelli, C. Padra, C.V. Turner, Shape optimization for tumor location, Comput. Math. Appl. 62 (11) (2011) 4068–4081.
[104] L. Jiang, W. Zhan, M.H. Loew, Modeling thermography of the tumorous human breast: from forward problem to inverse problem solving, in: 2010 IEEE International Symposium on Biomedical Imaging: From Nano to Macro, 2010, pp. 205–208.
[105] L. Jiang, W. Zhan, M.H. Loew, Toward understanding the complex mechanisms behind breast thermography: an overview for comprehensive numerical study, 2011, p. 79650H.
[106] U.R. Acharya, E.Y.K. Ng, J.-H. Tan, S.V. Sree, Thermography based breast cancer detection using texture features and support vector machine, J. Med. Syst. 36 (3) (2010) 1503–1510.
[107] J.M.Y. Tan, E.Y.K. Ng, R.A.U.L.G. Keith, J. Holmes, Comparative study on the use of analytical software to identify the different stages of breast cancer using discrete temperature data, J. Med. Syst. 33 (2) (2008) 141–153.
[108] S.V. Francis, M. Sasikala, S. Saranya, Detection of breast abnormality from thermograms using curvelet transform based feature extraction, J. Med. Syst. 38 (4) (2014) 23.